Calculations of Electron Inelastic Mean Free Paths (IMFPs). XIV. Calculated IMFPs for LiF and Si_3N_4 and Development of an Improved Predictive IMFP Formula

A. Jablonski[1], S. Tanuma[2,*] , and C. J. Powell[3]

[1] Institute of Physical Chemistry, Polish Academy of Sciences, ul. Kasprzaka 44/52, 01-224 Warsaw, Poland

[2] Materials Data Platform Center, National Institute for Materials Science, 1-1 Namiki, Tsukuba, Ibaraki 305-0044, Japan

[3]Associate, Materials Measurement Science Division, National Institute of Standards and Technology, Gaithersburg, MD 20899-8370, USA

Abstract

We report inelastic mean free paths (IMFPs) of Si_3N_4 and LiF for electron energies from 50 eV to 200 keV that were calculated from their optical energy-loss functions using the relativistic full Penn algorithm including the correction of the bandgap effect in insulators. Our calculated IMFPs, designated as optical IMFPs, could be fitted to a modified form of the relativistic Bethe equation for inelastic scattering of electrons in matter from 50 eV to 200 keV. The root-mean-square (RMS) deviations in these fits were less than 1 % for Si_3N_4 and LiF. The IMFPs were also compared with the relativistic version of our predictive Tanuma-Powell-Penn (TPP-2M) equation. We found that IMFPs calculated from the TPP-2M equation are systematically larger than the optical IMFPs for both LiF and Si_3N_4. The RMS differences between IMFPs from the TPP-2M equation and the optical IMFPs were 49.3 % for LiF and 17.3 % for Si_3N_4 for energies between 50 eV and 200 keV. These RMS differences are much larger than those for most of the inorganic compounds in our previous IMFP calculations where the average RMS difference was 10.7 % for 42 inorganic compounds. We also report the development of an improved predictive IMFP formula which we designate as the JTP equation. This formula is a refinement of the TPP-2M equation and is based on the recent IMFP calculations for 100 materials

* *Correspondence to*: Shigeo Tanuma, Materials Data Platform Center, National Institute for Materials Science, 1-1 Namiki, Tsukuba, Ibaraki 305-0044, Japan.
E-mail: Tanuma-sh@tbd.t-com.ne.jp and Tanuma.shigeo@nims.go.jp

including the present IMFPs for Si_3N_4 and LiF (41 elemental solids, 45 inorganic compounds, and 14 organic compounds) for 83 electron energies between 50 eV and 200 keV. Our predictive JTP equation gave satisfactory results in comparisons of optical IMFPs and IMFPs calculated from the JTP equation. The RMS difference between the 8300 optical IMFPs used for optimization and the IMFPs calculated from the JTP equation was 10.2 %. This value is appreciably less than the RMS difference of 16.0 % found in a similar comparison of the optical IMFPs and IMFPs from the TPP-2M equation. Furthermore, IMFPs from the JTP equation were compared with measured IMFPs for energies between 50 eV and 200 keV for 16 elemental solids and 37 inorganic compounds. We found that the JTP equation gave satisfactory results that were comparable to previous comparisons of the optical IMFPs and measured IMFPs. We believe that the JTP equation will be applicable to a wider range of materials than the TPP-2M equation.

1. Introduction

Information on the inelastic scattering of electrons in solids is important in various applications ranging from radiation physics to surface analysis by surface electron spectroscopies such as Auger electron spectroscopy (AES) and X-ray photoelectron spectroscopy (XPS). The most fundamental parameter in the latter applications is the electron inelastic mean free path (IMFP), λ, which is a useful measure of surface sensitivity. The IMFP is defined by ISO 18115[1] as the average distance that an electron with a given energy travels between successive inelastic collisions. The IMFP is simply related to the total cross-section for inelastic scattering and the number density of atoms per unit volume in the solid.

Tanuma *et al*. initially calculated IMFPs of 50 eV to 2,000 eV electrons for 27 elemental solids,[2,3] 15 inorganic compounds,[4] and 14 organic compounds[5] from energy-loss functions (ELFs) derived from experimental optical data. The IMFPs were calculated with the non-relativistic Penn algorithm[6] where the full Penn algorithm (FPA) was used for electron energies less than 200 eV and the single-pole approximation or simple Penn algorithm (SPA) was used for higher energies.

Tanuma *et al.* fitted their calculated IMFPs with a modified form of the Bethe equation[7] for inelastic scattering of electrons in matter and found that this equation with four parameters provided a good description of the IMFP dependence on electron energy for each material and for energies between 50 eV and 2000 eV. The average root mean square (RMS) differences between our calculated IMFPs (to be referred to later as optical IMFPs) and IMFPs from each fit were between 0.1 % and 1.0 % for the group of 27 elemental solids,[3] between 0.2 % and 1.0 % for the group of 15 inorganic compounds,[4] and between 0.2 % and 0.5 % for the group of 14 organic compounds.[5] The modified Bethe equation with the fit parameters found for each solid was thus a convenient analytical representation of the calculated IMFPs (e.g., for interpolation).

However, the early IMFP calculations for inorganic compounds were based on a limited set of optical data.[4] For many of the compounds, there were gaps in the available data for energy losses between 10 eV and 50 eV and it was necessary to interpolate the ELF values between these energies. The evaluations of these ELFs with two sum rules[8] showed that the resulting ELFs were unreliable.

As the early IMFP work progressed, Tanuma *et al*. developed a number of analytical expressions with which IMFPs could be estimated in any material.[2,3,5] These expressions were initially based on the fits of the calculated IMFPs to the original Bethe equation and later to the modified Bethe equation. They then analyzed the dependences of the fit parameters on various material parameters such as density, atomic or molecular weight, number of valence electrons per atom or molecule, and the bandgap energy for nonconductors. The latest

predictive formula[5] (designated TPP-2M and given as Equations (6) and (7) below) was based on the fits to the calculated IMFPs for the 27 elemental solids[3] and the 14 inorganic compounds[5] for electron energies between 50 eV and 2,000 eV. The average RMS difference between the optical IMFPs and IMFPs calculated from the TPP-2M equation was 10.2 % for the group of elemental solids and 8.5 % for the group of organic compounds.

Tanuma *et al.* made similar IMFP calculations for a group of 15 additional elemental solids, again for electron energies between 50 eV and 2,000 eV.[9] These IMFPs were compared with those from the TPP-2M equation. While satisfactory agreement between the calculated and predicted IMFPs for 12 of these solids, there were surprisingly large differences for Cs, diamond and graphite. These differences occurred for relatively small values of the parameter β in the TPP-2M equation for diamond and graphite and for relatively large values of β for Cs. Tanuma *et al.* believed that such extreme values of β were unlikely to be encountered for many other materials. Despite this limitation, the TPP-2M equation for estimating IMFPs in materials has been successfully employed in many applications.[10]

Tanuma *et al*. made additional IMFP calculations for another eight elemental solids and two compounds.[11] The main objective of this paper was to provide guidance on the appropriate choice for N_v, the number of valence electrons per atom or molecule in the TPP-2M equation.

The early IMFP calculations of Tanuma *et al*. have been extended in recent years by Shinotsuka *et al*. The latter authors employed a relativistic version of the full Penn algorithm to calculate IMFPs for a group of 41 elemental solids,[12] a group of 42 inorganic compounds,[13] and a group of 14 organic compounds and liquid water[14] for electron energies between 50 eV and 200 keV. Their calculations for the group of inorganic compounds were a significant improvement over the early work of Tanuma *et al*.[4] in that they used improved sets of optical data for some compounds and calculated optical data for some other compounds from the WIEN2k[15] and FEFF codes.[16] They also employed the algorithm of Boutboul *et al*.[17] to account for the bandgap energy of nonconductors.

An additional motivation for the work of Shinotsuka *et al*. was to provide IMFP data for so-called high-energy XPS (or HAXPES) and for transmission electron microscopy (TEM). In recent years, laboratory XPS instruments have been developed with X-ray sources for HAXPES experiments, with characteristic X-ray energies between 2 keV and 10 keV. In addition, HAXPES experiments have been conducted using synchrotron radiation with energies up to 15 keV. TEM experiments are routinely conducted with electron energies up to 200 keV.

Shinotsuka *et al.* [12,13,14] fitted their calculated IMFPs for each material with a modified relativistic form of the Bethe equation for inelastic electron scattering in matter. These fits, for

electron energies between 50 eV and 200 keV, were similar to those performed by Tanuma *et al*.[3-5] for electron energies between 50 eV and 2000 eV. Shinotsuka *et al.* found that the average RMS differences between IMFPs from the fits and the calculated IMFPs were 0.68 % for the group of elemental solids,[12] 0.60 % for the group of inorganic compounds,[13] and 0.17 % for the group of organic compounds and water.[14] The modified Bethe equation, with parameters from each fit, could then be used to describe the IMFP dependence on energy for each material, i.e., for interpolation.

Shinotsuka *et al*.[12] also developed a relativistic version of the TPP-2M equation. IMFPs from this equation were generally in agreement with the calculated IMFPs although relatively large differences were found for cubic BN (*c*-BN) and hexagonal BN (*h*-BN).[13] These large differences also occurred for relatively small values of the parameter β in the TPP-2M equation. The average RMS differences between the calculated IMFPs and IMFPs from the relativistic TPP-2M equation were 11.9 % for the group of 41 elemental solids, 10.7 % for the group of 42 inorganic compounds and 7.2 % for the group of 14 organic compounds and liquid water.

We report here the development of an improved predictive IMFP equation. This equation is a refinement of the TPP-2M equation and is based on the recent IMFP calculations of Shinotsuka *et al*.[12,13,14] for electron energies between 50 eV and 200 keV. Their IMFP calculations utilized the full Penn algorithm and the Boutboul *et al*.[17] algorithm for nonconductors. Before presenting the results of our analysis, however, we report new calculations of IMFPs for two inorganic compounds, LiF and Si_3N_4. These compounds were omitted from the Shinotsuka *et al*.[13] paper with IMFPs for inorganic compounds because reliable ELFs were not available at that time. The addition of IMFPs for LiF and Si_3N_4 was important for our analysis because these compounds have relatively large bandgap energies. Our new analysis is based on IMFP data for 100 substances: 41 elemental solids, 45 inorganic compounds, and 14 organic compounds.

2. IMFP Calculations for LiF and Si_3N_4

We calculated IMFPs for LiF and Si_3N_4 from their optical energy-loss functions (ELFs) with the relativistic full Penn algorithm[12] using the Boutboul *et al.* algorithm[17] that accounts for the bandgap energy in the IMFP calculations for nonconductors. The IMFP λ at an electron energy T can be calculated from:

$$\lambda(T)^{-1} = \frac{1}{\pi \cdot F(T - E_g) \cdot (T - E_g)} \iiint_D d\omega_p dq d\omega \frac{G(\omega_p)}{q} \mathrm{Im}\left[\frac{-1}{\varepsilon_L(q, \omega, \omega_p)}\right], \qquad (1)$$

where E_g is the bandgap energy, ε_L denotes the Lindhard dielectric function[18] of a free-electron gas with plasmon energy $\omega_p\left(=\sqrt{4\pi n}\right)$, n is the electron density, q is the momentum transfer, ω is the energy loss,

$$F(T) = \left(1 + \frac{T}{2c^2}\right) / \left(1 + \frac{T}{c^2}\right)^2, \tag{2}$$

$$G(\omega) = \frac{2}{\pi\omega} \mathrm{Im}\left[\frac{-1}{\varepsilon(\omega)}\right], \tag{3}$$

$$D = \left\{\left(\omega, q, \omega_p\right) | E_g \le \omega \le \left(T - E_g - E_v\right),\ q_- \le q \le q_+ , 0 < \omega_p < \infty\right\}, \tag{4}$$

$$q_\pm = \sqrt{T\left(2 + T\right)/c^2)} \pm \sqrt{(T - \omega)\left[2 + (T - \omega)/c^2\right]}, \tag{5}$$

c is the speed of light, E_v is the width of valence band, and $\mathrm{Im}[-1/\varepsilon(\omega)]$ is the optical ELF. We use Hartree atomic units ($m_e = e^2 = \hbar = 1$) where m_e is the electron rest mass, e is the elementary charge, and $\hbar$ is the reduced Planck constant.

The material-property data used in the IMFP calculations for LiF and Si_3N_4 and in the analysis of ELFs and IMFPs are the molecular weight M: 25.938 and 140.283, density ρ: 2.64 g/cm^3 and 3.17 g/cm^3, number of valence electrons per molecule N_v: 8 and 32, bandgap energy E_g: 12.6 eV and 5.0 eV, and valence-band width E_v: 6.0 eV and 9.7 eV, respectively.

2.1 Optical energy-loss functions and their evaluations

Table 1 shows the sources of optical data used in the IMFP calculations for LiF and Si_3N_4. For LiF, we calculated optical constants from the WIEN2k and FEFF codes as described previously.[13]

We checked the internal consistency of our ELF data for each compound with the oscillator-strength or f-sum rule and a limiting form of the Kramers-Kronig integral (or KK-sum rule).[19] The values of the f-sum and KK-sum rules for LiF were 12.8 (error: 6.9 %, theoretical value: 12) and 1.09 (error: 9 %, theoretical value: 1), respectively. The corresponding values for Si_3N_4 were 72.2 (error: 3.1 %, theoretical value: 70) and 1.025 (error: 2.5 %), respectively. The values of the f-sum error for these two compounds (6.9 % and 3.1 %) are similar to the average f-sum error (4.1%) found for our group of 42 inorganic compounds.[13] The values of the KK-sum error for Si_3N_4 (3.1 %) is less than the average KK-sum error for

the group of 42 inorganic compounds (3.5 %) while that for LiF (9 %) is larger. However, the errors are less than 10 % which is the limit that we have set previously.[13] We also point out that the errors in the KK-sum rule for the ELF data of LiF and Si_3N_4 used by Tanuma *et al*.[4] for their early IMFP calculations were 30 % (LiF) or more (Si_3N_4).

2.2 IMFP results and Analysis of IMFPs

We show the calculated IMFPs for LiF and Si_3N_4 in Table 2 as a function of electron kinetic energy E with respect to the bottom of the conduction band for energies between 50 eV and 200 keV. These IMFPs are plotted as solid circles in Figs. 1(A) and 1(B). Calculated IMFPs are also included in Figs. 1(A) and 1(B) for energies less than 50 eV and over 200 keV to illustrate trends. The IMFPs for energies less than 50 eV, however, are not considered as reliable as those at energies between 50 eV and 200 keV.[2,12] We also note that the calculated IMFPs for energies larger than 200 keV must be slightly larger than the true values because we neglected the contribution of the transverse term in the differential cross section for inelastic scattering.[12]

The relativistic modified Bethe equation used in our analysis is:[12]

$$\lambda(E) = \frac{\alpha(E)E}{E_{\mathrm{p}}^2\{\beta[\ln(\gamma\alpha(E)E)] - (C/E) + (D/E^2)\}}, \qquad \text{(nm)} \qquad (6a)$$

where

$$\alpha(E) = \frac{1 + \frac{E}{(2m_e c^2)}}{\left[1 + \frac{E}{(m_e c^2)}\right]^2} \approx \frac{1 + E/1021999.8}{(1 + E/510998.9)^2}, \qquad (6b)$$

$$E_{\mathrm{p}} = 28.816\left(\frac{N_{\mathrm{v}}\rho}{M}\right)^{0.5}, \qquad \text{(eV)} \qquad (6c)$$

and E is the electron kinetic energy (in eV) above the bottom of the conduction band, ρ is the bulk density (in g cm^{-3}), N_{v} is the number of valence electrons per atom or molecule, M is the atomic or molecular weight, and β, γ, C, and D are parameters.

The relativistic TPP-2M equation consists of Eq. (6) and the following equations for the four parameters:[12]

$$\beta = -1.0 + \frac{9.44}{\left(E_{\mathrm{p}}^2 + E_{\mathrm{g}}^2\right)^{0.5}} + 0.69\rho^{0.1} \quad (\mathrm{eV}^{-1}\mathrm{nm}^{-1}) \qquad (7a)$$

$$\gamma = 0.191\rho^{-0.5} \qquad (\mathrm{eV}^{-1}) \qquad (7b)$$

$$C = 19.7 - 9.1U \qquad (\mathrm{nm}^{-1}) \qquad (7c)$$

$$D = 534 - 208U \qquad (\mathrm{eV\ nm}^{-1}) \qquad (7d)$$

$$U = \frac{N_{\mathrm{v}}\rho}{M} = \left(\frac{E_{\mathrm{p}}}{28.816}\right)^2 \qquad (7e)$$

The triangles in Figs. 1(A) and 1(B) show IMFPs from the earlier calculations of Tanuma *et al*.[4] The IMFPs for LiF are generally smaller than the new values while those for Si_3N_4 are larger. We also show IMFPs calculated from the relativistic TPP-2M equation (long-dashed lines) and fits (solid lines) to the calculated IMFPs with the modified Bethe equation [Eq. (6)] for energies between 50 eV and 200 keV. Table 3 shows values of the parameters in these fits for each compound as well as values of the average RMS differences, *RMS*, between the fitted IMFPs and the optical IMFPs. Finally, Figures 1(A) and 1(B) show IMFPs from the JTP equation to be described in Section 4.

Figures 1(C) and 1(D) show ratios of IMFPs from the earlier IMFP calculations, the TPP-2M equation, the fits with the modified Bethe equation, and the JTP equation to the optical IMFPs for LiF and Si_3N_4 as a function of electron energy for energies between 50 eV and 200 keV. For LiF, there is good agreement in Fig. 1(C) between the previous IMFPs and the new IMFPs for energies between 500 eV and 2000 eV where the differences are less than 1 %. For lower energies, however, the previous IMFPs are smaller than the new IMFPs with decreasing energy. These changes must be due in part to differences in the ELFs used for the two calculations. In addition, our previous IMFP calculations for LiF did not account for the bandgap energy. However, for materials with a large bandgap energy such as LiF, this parameter is expected to have a significant effect on the IMFPs only for energies less than about 50 eV.[13] Figure 1(C) also shows that IMFPs from the TPP-2M equation for LiF are substantially larger than the optical IMFPs. The average RMS deviation between the TPP-2M IMFPs and the optical IMFPs was 49.3 % for energies between 50 eV and 200 keV.

For Si_3N_4, Fig. 1(D) shows that the previous IMFPs are systematically larger than the new IMFPs by about 20 % for energies between 100 eV and 2000 eV. This change is mainly due to differences between the previous and new ELFs. The new ELF was obtained from a first-principles calculation as described in Section 2.1. Comparison of the previous and new ELFs showed that there was a large difference in ELF intensities in the 20 to 30 eV energy-loss range. The peak intensity of the new ELF was about 1.7 times larger than that of the previous ELF. This increase is considered reasonable in view of the improved values of the KK-sum rule shown in Section 2.1. As a result, IMFPs calculated from the previous ELF are generally larger than the new IMFPs.

Figure 1 also shows that the fits with the modified Bethe equation are in excellent agreement with the optical IMFPs for both LiF and Si_3N_4 for energies between 50 eV and 200 keV. The average RMS differences between IMFPs from the fits and the optical IMFPs were 0.85 % for LiF and 0.6 % for Si_3N_4. The maximum difference was less than 3 % for LiF and less than 1 % for Si_3N_4. We also see that IMFPs calculated from the TPP-2M equation are systematically larger than the optical IMFPs for both LiF and Si_3N_4. The average RMS

differences between IMFPs from the TPP-2M equation and the optical IMFPs were 49.3 % for LiF and 17.3 % for Si_3N_4 for energies between 50 eV and 200 keV. These differences are much larger than those for most of the inorganic compounds in our previous IMFP calculations[13] where the RMS difference between IMFPs from the TPP-2M equation and the optical IMFPs was 10.7 %. The improved result from the JTP equation will be described in Section 4.

3. Development of an improved predictive IMFP equation

3.1 Optimization strategy for the new predictive IMFP equation

We analyzed the IMFPs calculated by Shinotsuka *et al.* for 100 materials (41 elemental solids[12], 44 inorganic compounds[13], 14 organic compounds and liquid water[14]) that were calculated with the full Penn algorithm and with the Boutboul *et al*. approach[17] for nonconductors. These calculations were made with what we consider to be reliable ELFs, as judged by evaluations with the two sum rules described in Section 2.1. The IMFPs were calculated at 83 energies between 50 eV and 200 keV. Using this data set, we developed a new predictive IMFP equation. The new equation is based on the structure of the TPP-2M equation which was based on the modified Bethe equation.[5]

Limitations of the TPP-2M equation for some materials have been pointed out,[9, 13] as summarized in Sections 1 and 2.2. Figure 2 shows a rank-order diagram for values of RMS_i, the average RMS percentage difference between IMFPs, $\lambda_i^{cal}(E_j)$, from the TPP-2M equation for material i and the corresponding optical IMFPs, $\lambda_i^{optical}(E_j)$, for 83 values of the energy, E_j. Values of RMS_i were calculated for each of the 100 materials from:

$$\mathrm{RMS}_i = 100 \times \left[\sum_{j=1}^{83} \left(\frac{\lambda_i^{cal}(E_j) - \lambda_i^{optical}(E_j)}{\lambda_i^{optical}(E_j)} \right)^2 /83 \right]^{0.5} .(\%) \qquad (8)$$

These values were then arranged in ascending order with RMS_i plotted as a function of the rank order in Fig. 2.

As shown in Fig. 2, six materials (diamond, *c*-BN, LiF, graphite, Cs, and *h*-BN) had RMS_i values larger than 30 %. We found that the large values of RMS_i for these six materials occurred for unusually small or large values of the parameter β in the TPP-2M equation [from Eq. (7b)].[13] We also note that inorganic materials, including some with large bandgap energies (such as Al_2O_3 and LiF) were not included in the original development of the TPP-2M equation. Nevertheless, Fig. 2 shows that the values of RMS_i were less than 20 % for about 90 % of our materials and were less than 10 % for 67 % of the materials. Despite its limitations, the TPP-

2M equation has been useful for providing estimates of IMFPs for many materials.

The four parameters β, γ, C, and D in the TPP-2M equation were determined by fitting the optical IMFPs of 27 elemental solids and 14 organic compounds for energies between 50 eV and 2 keV with the modified Bethe equation.[5] These fits were made using values of four material properties (ρ, M, E_g, and N_v) and led to the predictive equations shown in equation (7). These expressions were optimized by calculating the value of RMS_i for each material and minimizing the average of the RMS_i values.

We report here the development of an improved predictive IMFP formula. Our goal in this work was to reduce the number of materials with large values of RMS_i, i.e., to minimize the maximum value of $RMSi$. We started with the following generalized expressions for the four parameters in the TPP-2M equation:

$$\beta = \frac{c_1}{\left(E_p^2 + E_g^2\right)^{c_2}} - c_3 + c_4\rho^{c_5} \qquad \left(\mathrm{eV}^{-1}\ \mathrm{nm}^{-1}\right), \tag{9a}$$

$$\gamma = c_6\rho^{-c_7}, \qquad \left(\mathrm{eV}^{-1}\right) \tag{9b}$$

$$C = c_8 - c_9U, \qquad \left(\mathrm{nm}^{-1}\right) \tag{9c}$$

$$D = c_{10} - c_{11}U, \qquad \left(\mathrm{eV\ nm}^{-1}\right) \tag{9d}$$

where the terms c_1 to c_{11} are parameters to be varied in the optimization.

Our goal was to derive an improved predictive IMFP equation by optimization of an appropriate expression. We decided to minimize the sum of squared relative IMFP differences, S:

$$S = \sum_{i=1}^{m_{tot}} \sum_{j=1}^{n} (\Delta_{ij})^2 , \tag{10a}$$

where

$$\Delta_{ij} = \frac{\lambda_i^{fit}\left(E_j\right) - \lambda_i^{optical}\left(E_j\right)}{\lambda_i^{optical}\left(E_j\right)} , \tag{10b}$$

and λ_i^{fit} is calculated from Eqs. (6a) to 6(c) with the newly optimized parameters expressed by Eqs. (9a) to (9d). The summation in Eq. (10a) was made over the 100 materials and 83 energies (i.e., 8300 values) of our data set of optical IMFPs for energies between 50 eV and 200 keV from the calculations of Shinotsuka *et al.*[12,13,14] and from the calculated IMFPs for LiF and Si_3N_4 presented here. From the final optimized value of the function S, we can determine the corresponding total RMS percentage difference, RMS_{total}:

$$RMS_{total} = 100 \times \left(\frac{S}{100 \times 83}\right)^{0.5} = 100 \times \left[\frac{1}{100}\sum_{i=1}^{100}\left(\frac{1}{83}\sum_{j=1}^{83}(\Delta_{ij})^2\right)\right]^{0.5}$$

$$= \left[\frac{1}{100}\sum_{i=1}^{100}(RMS_i)^2\right]^{0.5}. \qquad (10c)$$

In this way, the weight of the optimization will be applied to materials with the largest RMS_i values. Consequently, the maximum RMS_i values are expected to become smaller.

Values of λ_i^{fit} were determined from Eqs. (6) and (9) for each material and energy at each stage of the optimization. The parameters c_1 to c_{11} were then adjusted in attempts to minimize the value of RMS_{total}. We note here that $c_2 = 0.5$ was fixed in the TPP-2M equation shown in Eq. (7a).

A number of attempts were made to find an optimal approach for minimization of RMS_{total}. The successful approach consisted of two stages. First, after an initial selection of values for the parameters c_1 to c_{11}, the Monte Carlo method was used to locate a prospective region in multi-parameter space for minimization. This method is known as random search and is ascribed to Rastrigin.[20] Second, refinement of an initial minimum position in multi-parameter space was made using the direction set method.[21]

3.2 Additional criteria for evaluation of the new predictive IMFP equation

We utilized several additional criteria in our evaluations of the new predictive IMFP equation. In the equations given below, the subscripts i and j are indexes referring to the material and the electron energy, respectively.

The RMS difference between the optical IMFPs and IMFPs calculated from the proposed new predictive IMFP formula or from the TPP-2M equation can be calculated for the group of elemental solids (m = 41), the group of inorganic compounds (m = 45), the group of organic compounds (m = 14), and for all materials (m = 100) from:

$$RMS_x = \left[\frac{1}{m}\sum_{i=1}^{m}(RMS_i)^2\right]^{0.5}, \qquad (11)$$

where the subscript x represents one of the groups of materials [i.e., elemental solids (elem), inorganic compounds (inorg), or organic compounds (org)], or to all materials (total) in our IMFP data set. Values of RMS_i in Eq. (11) were obtained from Eq. (8).

The average of the RMS_i values for a material group x that contains m materials, $< RMS_i >_x$, is calculated from

$$< RMS_i >_x = \frac{1}{m}\sum_{i=1}^{m} RMS_i \,. \tag{12}$$

In the summation of Eq. (12), the number of materials m is 100 for all materials in our data set (total), m = 41 for the group of elemental solids, m = 45 for the group of inorganic materials, and m = 14 for the group of organic compounds.

The median and maximum values of RMS_i for the material group x that contains m materials, $\left[RMS_i\right]_x^{med}$ and $\left[RMS_i\right]_x^{max}$, are given by

$$\left[RMS_i\right]_x^{med} = \underset{1 \le i \le m}{\text{Median}}\left[RMS_i\right] \text{ and} \tag{13}$$

$$\left[RMS_i\right]_x^{max} = \underset{1 \le i \le m}{\text{Max}}\left[RMS_i\right], \tag{14}$$

respectively.

We also determined the mean of the absolute percentage differences between the IMFPs from the new equation and our optical IMFPs for the material group x that contains m materials:

$$< P_i >_x = \frac{1}{m}\sum_{i=1}^{m} P_i = 100\frac{1}{m}\sum_{i=1}^{m}\left(\frac{1}{83}\sum_{j=1}^{83}\left|\Delta_{ij}\right|\right), \tag{15}$$

where Δ_{ij} is obtained from Eq. (10b). The maximum absolute percentage difference between the IMFPs from the new equation and the optical IMFPs for material i, $\left[P_i\right]^{max}$, is given by

$$\left[P_i\right]^{max} = \underset{1 \le j \le 83}{\text{Max}}\left[100 \times \left|\Delta_{ij}\right|\right]. \tag{17}$$

A useful measure for the quality of a fit is the maximum value of P_i for the material group x, $\left[P_i\right]_x^{max}$, that contains m materials:

$$\left[P_i\right]_x^{max} = \underset{1 \le i \le m, 1 \le j \le 83}{\text{Max}}\left[100 \times \left|\Delta_{ij}\right|\right]. \tag{18}$$

4. Results

4.1 New Predictive Equation for IMFPs between 50 eV and 200 keV

We obtained the following equations from the minimization of RMS_{total} from Eq. (10) using the calculated IMFPs of Shinotsuka *et al*. for 100 materials and 83 energies as reference values:

$$\lambda(E) = \frac{\alpha(E)E}{E_{\mathrm{p}}^2\left\{\beta[\ln(\gamma\alpha(E)E)] - (C/E) + \left(D/E^2\right)\right\}}, \qquad \text{(nm)} \qquad (19a)$$

$$\beta = 0.0539 + \frac{17.0}{\left(E_p^2 + E_g^2\right)^{0.639}} - 0.252\rho^{-0.463}, \qquad \left(\mathrm{eV}^{-1}\ \mathrm{nm}^{-1}\right) \qquad (19b)$$

$$\gamma = 0.115\ \rho^{-0.253}, \qquad \left(\mathrm{eV}^{-1}\right) \qquad (19c)$$

$$C = 9.76 + 2.09\ U, \qquad \left(\mathrm{nm}^{-1}\right) \qquad (19d)$$

and

$$D = 97.5 + 223U\ . \qquad \left(\mathrm{eV\ nm}^{-1}\right) \qquad (19e)$$

Equations (6) and Equation (19) represent our new predictive IMFP equation that will now be referred to as the JTP equation.

The value of RMS_{total} from Eq. (10) was 10.2 %. This value is smaller than the corresponding value (16 %) for the TPP-2M equation. We show the rank-order diagram for the RMS_i values from the present analysis (indicated by JTP) in Fig. 2 where they are compared with the RMS_i values from the TPP-2M equation. We see that the RMS_i plots are essentially identical for RMS_i values less than 15 %. The big difference between the plots is that the large RMS_i values found from the TPP-2M equation for diamond, graphite, Cs, LiF, *h*-BN, and *c*-BN are now appreciably reduced with the JTP equation. We have therefore succeeded in our goal of finding a new predictive IMFP equation that does not give excessively large RMS_i values.

The correlation between the RMS_i values from the two equations for each of the 100 materials is shown in Figure 3. From this figure, we see that the three inorganic compounds (*c*-BN, *h*-BN, and LiF) and the three elemental solids (diamond, graphite, and Cs) that had large RMS_i values with the TPP-2M equation have much smaller RMS_i values with the JTP equation. In other words, the six materials with RMS_i values between 30 % and 70 % with the TPP-2M equation have RMS_i values of approximately 20 % or less with the JTP equation. The JTP equation is thus a more generally useful IMFP predictive formula. We also conclude that our use of Eq. (10a) for optimization was effective.

4.2 Evaluations of the JTP predictive IMFP equation

4.2.1 Additional results from the optimization

Table 4 shows values of the parameters listed in Section 3.2 for evaluations of IMFPs from the JTP equation and from the TPP-2M equation. This Table includes not only results for all 100 materials but also separate results for the 41 elemental solids, 45 inorganic compounds, and 14 organic compounds. We make comparisons first for electron energies between 50 eV and 200 keV and will later consider the smaller energy range of 200 eV to 200 keV.

In our series of IMFP papers[12,13,14], we have used $<RMS_i>_x$ from Eq. (12), the average RMS_i value for each group of materials x, as an indicator of the extent to which IMFPs from the TPP-2M equation agree with the corresponding optical IMFPs. We see from Table 4 that $<RMS_i>_{total}$ was 11.1 % for IMFPs from the TPP-2M equation and 8.7 % for IMFPs from the JTP equation, a 28 % decrease. The largest difference in $<RMS_i>_x$ values between the two equations was in the group of inorganic compounds where $<RMS_i>_{inorg}$ was 8.5 % and 11.6 % for the JTP and TPP-2M equations, respectively. For the group of elemental solids, $<RMS_i>_{elem}$ was 9.6 % and 11.9 % for IMFPs from the JTP and TPP-2M equations, respectively, while for the group of organic compounds $<RMS_i>_{org}$ was 6.8 % and 7.1 % for IMFPs from the JTP and TPP-2M equations, respectively. Satisfactory $<RMS_i>_x$ results were thus obtained for IMFPs from the JTP equation for all three groups of materials.

The metrics in Table 4 that showed the largest differences between the JTP and TPP-2M equations were $\left[RMS_i\right]_{total}^{max}$ and $\left[P_i\right]_{total}^{max}$. The former metric is the maximum value of RMS_i among all materials and the latter is the absolute value of the maximum relative difference for a material i and energy j. Both quantities give information not recognizable from the average value of RMS_i and the mean absolute deviation $<P_i>$. For the TPP-2M equation, $\left[RMS_i\right]_{total}^{max}$ is 70.6 % and $\left[P_i\right]_{total}^{max}$ is 75 % (both values are for diamond). For the JTP equation, however, $\left[RMS_i\right]_{total}^{max}$ is 23.7 % and $\left[P_i\right]_{total}^{max}$ is 36.0 %. The latter two values are much less than the corresponding values for the TPP-2M equation.

For a more complete description of our results, we now show values of RMS_i (the average RMS percentage difference between IMFPs calculated from a predictive IMFP formula and the optical IMFPs for material i) and of P_i^{max} (the largest absolute percentage difference between IMFPs from a predictive IMFP formula and the optical IMFPs for material i). Tables 5, 6, and 7 show values of these metrics for each material in our groups of 41 elemental solids, 45 inorganic compounds, and 14 organic compounds, respectively.

4.2.2 Comparisons of IMFPs from the JTP and TPP-2M equations

Figures 4(A) and 4(B) show plots of ratios of IMFPs calculated from the JTP equation [Equations 6 and 19] and from the TPP-2M equation [Equations 6 and 7] to the corresponding optical IMFPs for the 100 materials as a function of electron energy between 50 eV and 200

keV. These plots enable visual assessments of the reliability of each equation. Ideally, these ratios should be close to unity and not change with energy.

The ratios for the JTP equation in Fig. 4(A) for each material are nearly constant for energies between about 500 eV and 200 keV but there are often substantial changes at lower energies (typically for energies less than about 200 eV). For energies above 500 eV, most ratios are approximately constant with energy at values between 0.8 and 1.2. Most ratios for the TPP-2M equation in Fig. 4(B) are also approximately constant with energy for energies between 300 eV and 200 keV and these ratios also have values between approximately 0.8 and 1.2. However, there are six materials (diamond, *c*-BN, LiF, graphite, *h*-BN, and Cs) with ratios above 1.3. Among these, diamond shows the largest ratio, above 1.7, for energies between 100 eV and 200 keV. For energies below 200 eV, the ratios in Figs. 4(A) and 4(B) show more variability from material to material. We therefore evaluated the metrics in Table 4 for energies between 200 eV and 200 keV. As expected from Figs. 4(A) and 4(B), the values of these metrics are typically smaller than those for the 50 eV to 200 keV energy range.

We now consider the RMS percentage difference between IMFPs from either the JTP or TPP-2M equations and the optical IMFPs, RMS_j, at a particular energy for a group of materials (elemental solids, inorganic compounds, organic compounds, or all materials):

$$RMS_j = 100 \times \left[\sum_{i=1}^{n} \left(\frac{\lambda_i^{cal}(E_j) - \lambda_i^{optical}(E_j)}{\lambda_i^{optical}(E_j)} \right)^2 / n \right]^{0.5} .(\%) \qquad (20)$$

The solid line in Fig. 4(C) shows RMS_j, for the JTP equation and for all materials as a function of electron energy. This plot is almost constant for energies between 150 eV and 200 keV with an average value of 10.0 %. At lower energies, RMS_j, increases from 10.5 % at 148 eV to 12.4 % at 54 eV. In contrast, the RMS_j values for the TPP-2M equation exceed 15 % for all energies, with a maximum value of 17.1 % at around 90 eV. Above 100 eV, RMS_j decreases almost uniformly with increasing electron energy and reaches a value of 15.4 % at 200 keV.

We also show the energy dependence of RMS_j values from the JTP and TPP-2M equations in Figs. 4(C) and 4(D) for each group of materials. For the elemental solids and inorganic compounds, the energy dependences of RMS_j are similar to the corresponding plots for all materials. That is, *RMSj* does not change significantly with electron energy. However, the values of *RMSj* for organic compounds are smaller than those for elemental solids over the entire energy range for both equations. We also point out that the RMS_j values for the JTP equation for elemental solids and inorganic compounds at 992.3 eV are 10.9 % and 9.5 %, respectively, while those for the TPP-2M equation are 17.7 % and 16.5 %, an increase of about

60 %.

The energy dependence of the RMS_j values from the TPP-2M equation for the organic compounds is distinctly different from that for the elemental solids and inorganic compounds. We also note that these RMS_j values are roughly equal to those from the JTP equation for energies between 200 eV and 200 keV. For example, RMS_j from the TPP-2M equation is 7.4 % at 992.3 eV while RMS_j from the JTP equation is 7.0 %. Both equations thus provide useful estimates of the IMFPs of organic compounds for energies between 200 eV and 200 keV.

4.3 Analysis of the β and γ terms in the JTP and TPP-2M equations

The 11 parameters in Eq. (9) were optimized by use of Eq. (10) to yield our JTP equation [Eq. (19)] for estimating IMFPs. As described in Section 3, we minimized the sum of squares of relative differences between the calculated IMFPs for 100 materials (41 elemental solids, 45 inorganic compounds, and 14 organic compounds) at 83 energies between 50 eV and 200 keV (our optical IMFPs) and the IMFPs from Eq. (9) as shown in Eq.(10a). In contrast, the parameters in the earlier TPP-2M predictive IMFP equation [Eq. (7)] were derived from fits of calculated IMFPs for 27 elemental solids and 15 organic compounds at 22 energies between 50 eV and 2000 eV to the nonrelativistic form of the modified Bethe equation [Eq. (6)]. Expressions were obtained for the four parameters in Eq. (6a) (β, γ, C, and D) in terms of four material properties (bulk density, atomic or molecular weight, number of valence electrons per atom or molecule, and bandgap energy (for nonconductors)), as shown in Eqs. (7a), 7(b), 7(c), and 7(e). Different expressions for these parameters were derived for the JTP equation in terms of the same material properties, as shown in Eqs. (19b), (19c), (19d), and 19(e).

IMFPs from the JTP and TPP-2M equations for a given electron energy are mainly determined by the values of β and γ for energies above 200 eV since the contributions of the C and D terms are relatively small at these energies. We have therefore evaluated the values of β and γ from each predictive IMFP equation for a given material, which we designate as β_{JTP} and γ_{JTP} for the JTP equation and $\beta_{\mathrm{TPP\text{-}2M}}$ and $\gamma_{\mathrm{TPP\text{-}2M}}$ for the TPP-2M equation. We have also made comparisons of these parameters with the corresponding values of β and γ, β_{fit} and γ_{fit}, found in the fits of the calculated IMFPs to the modified Bethe equation [Eq. (6a)] for each of our 100 materials at energies between 50 eV and 200 keV, as shown in Refs. 12 to 14 and Table 3. These comparisons are useful because of the significant differences in how the parameters in the JTP and TPP-2M equations were determined.

Figure 5 shows the γ values versus the β values for (A, B) the modified Bethe equation, (C, D) the JTP equation, and (E, F) the TPP-2M equation. In Figures 5(A), (C), and (E), we see that the alkali metals (Li, Na, K, Cs) show much larger β values than for the other materials. Furthermore, the value of β for the alkali metals increases at an approximately constant rate

with increasing atomic number in the three equations. Figures 5(B), (D) and (F) also show that the range of β values occupy approximately the same range except for the alkali metals with each equation. That is, the β values are concentrated in a narrow range between about 0.1 and 0.7. The fact that the four "outlier" points in each plot are for the alkali metals suggests that the optical ELFs for these elements might have greater uncertainty than for the other elemental solids. The alkalis are very reactive, and it is perhaps likely that their surfaces had some oxide during the optical measurements even though their optical ELFs satisfied our sum-rule tests.[9] Further checks on the ELFs of the alkali metals would be desirable.

On the other hand, there are large differences in the γ values found for each equation as shown in Figures 5(A), 5(C) and 5(E). In particular, the $\gamma_{\rm fit}$ values for the alkali metals from the modified Bethe equation in Figure 5(A) are significantly larger than those for the other materials. In particular, the value of γ_{fit} for Li is 0.44, a value which is more than twice those for the other materials. A noteworthy result of the JTP equation is that the γ_{JTP} values for the alkali metals are less than the corresponding γ_{fit} values, as shown in Figures 5(A) and 5(C). In other words, the range of the $\gamma_{\rm JTP}$ values for all materials, between 0.05 and 0.14, is much smaller than the corresponding ranges of $\gamma_{\rm fit}$ in Fig. 5(B) (between 0.04 and 0.18) and of $\gamma_{\rm TPP\text{-}2M}$ in Fig. 5(F) (between 0.04 and 0.2) with the exclusion of data for the alkali metals in each comparison. We have no explanation for this result.

Figure 6(A) show values of $\beta_{\rm JTP}$ from Eq. (19b) for our 100 materials as a function of the corresponding values of $\beta_{\rm fit}$. A similar plot is given in Fig. 6(B) of $\beta_{\rm TPP\text{-}2M}$ values from Eq. (7a) as a function of $\beta_{\rm fit}$. The solid lines in each plot indicate perfect correlation between the β values from each equation and $\beta_{\rm fit}$ while the dashed lines indicate β values that are 20 % larger or smaller than the values for the solid line. There are no appreciable differences in the β values from the two equations except for $\beta_{\rm fit} < 0.2$. However, there are six materials (diamond, graphite, *c*-BN, *h*-BN, MgF_2 and LiF) that have $\beta_{\rm TPP\text{-}2M}$ values 20 % less than $\beta_{\rm fit}$. In contrast, there are no materials for which $\beta_{\rm JTP}$ is smaller than $0.8\beta_{\rm fit}$.

The β parameter is always used in IMFP calculations with the TPP-2M and JTP equations as a product with E_p^2 as shown in Equations (6) and (19a). We therefore show values of $E_p^2\beta_{\rm JTP}$ and $E_p^2\beta_{\rm TPP\text{-}2M}$ for our 100 materials in Figures 6(C) and 6(D) as a function of the corresponding $E_p^2\beta_{\rm fit}$ values. The alkali-metal group, which in Figure 6(A) showed very large β values compared to the other materials, now has smaller $E_p^2\beta$ values than the other materials in Fig. 6(C). However, these values are not significantly smaller than those of the other materials. In other words, there was generally a good correlation between $E_p^2\beta_{\rm JTP}$ and $E_p^2\beta_{\rm fit}$ for the 100 materials. In the case of the TPP-2M equation, a linear scale plot as shown in Fig. 6(D) shows more clearly than in Fig. 6(B) that the $E_p^2\beta_{\rm TPP\text{-}2M}$ values for the six materials are clearly smaller than the corresponding $E_p^2\beta_{\rm fit}$ values.

Figure 6(E) shows a plot of the average RMS percentage differences between IMFPs from the JTP equation and the optical IMFPs for each of our 100 materials, RMS_i, from Eq. (8) as a function of β_{JTP}/β_{fit}. A similar plot for RMS_i values from the TPP-2M equation is given in Fig. 6(F). We see that the RMS_i values for IMFPs from the JTP equation correlate roughly with the ratio β_{JTP}/β_{fit} in Fig. 6(E). There is also a similar correlation of the RMS_i values for IMFPs from the TPP-2M equation with the ratio $\beta_{TPP\text{-}2M}/\beta_{fit}$ in Fig. 6(F). For values of β/β_{fit} between 0.8 and 1.2, both equations show very similar trends: the RMS_i values reach a minimum when β_{JTP}/β_{fit} or $\beta_{TPP\text{-}2M}/\beta_{fit}$ is near unity. The RMS_i values then increase for smaller or larger values of β_{JTP}/β_{fit} and $\beta_{TPP\text{-}2M}/\beta_{fit}$.

There are six materials in Fig. 6(F) (diamond, graphite, *c*-BN, *h*-BN, MgF_2, and LiF) for which $\beta_{TPP\text{-}2M}/\beta_{fit} < 0.8$. Five of them have RMS_i values between 30 % and 70 % while the RMS_i value for MgF_2 is 19.3 %. We also note that the RMS_i value for Cs is 35 % although $\beta_{TPP\text{-}2M}/\beta_{fit}$ for Cs is 0.82 (slightly larger than 0.8). In contrast, there are no materials in Fig. 6(E) with $\beta_{JTP}/\beta_{fit} < 0.8$ and no materials with RMS_i values larger than 25 %. We conclude that materials with $\beta_{TPP\text{-}2M}/\beta_{fit} < 0.8$ could yield IMFPs from the TPP-2M equation with larger uncertainties than if this ratio was larger than 0.8. However, this limitation does not apply to the corresponding ratio (β_{JTP}/β_{fit}) for the JTP equation.

We note that IMFPs for diamond, *c*-BN, *h*-BN, MgF_2, and LiF were not included in the development of the TPP-2M equation. Furthermore, these materials have relatively large bandgap energies and their electronic properties are very different from those of the 27 elemental solids and 15 organic compounds that were considered in the development of the TPP-2M equation.[5] As a result, it is not surprising that IMFPs from the TPP-2M equation would have large uncertainties for materials with large bandgap energies.

Figure 7(A) is a plot of γ_{JTP} from Eq. (19c) for our 100 materials (symbols) as a function of the corresponding values of γ_{fit}. A similar plot is given in Fig. 7(B) of $\gamma_{TPP\text{-}2M}$ values from Eq. (7b) as a function of γ_{fit}. While there is a rough proportionality between the $\gamma_{TPP\text{-}2M}$ and γ_{fit} values in Fig. 7(B), many of the plotted points have $\gamma_{TPP\text{-}2M}$ values less than 20 % of the corresponding γ_{fit} values. In contrast, the γ_{JTP} values in Fig. 7(A) show a much weaker dependence on γ_{fit} than for the plot of $\gamma_{TPP\text{-}2M}$ versus γ_{fit} in Fig. 7(B).

The parameter γ is used to form the product $E_p^2\beta\ln(\gamma)$ in the IMFP calculation, as shown in Equation (19a). We therefore show $E_p^2\beta_{fit}\ln(\gamma_{JTP})$ in Fig. 7(C) and $E_p^2\beta_{fit}\ln(\gamma_{TPP-2M})$ in Fig. 7(D) as a function of $E_p^2\beta_{fit}\ln(\gamma_{fit})$ for the JTP equation and TPP-2M equation, respectively. We see that the plotted points in Figs. 7(C) and 7(D) vary roughly linearly with $E_p^2\beta_{fit}\ln(\gamma_{fit})$.

Figure 7(E) shows a plot of the RMS_i values in comparisons of IMFPs from the JTP equation and the optical IMFPs for each of our 100 materials from Eq. (8) as a function of

$\gamma_{JTP}/\gamma_{fit}$. A similar plot of RMS_i values in comparisons of IMFPs from the TPP-2M equation with the optical IMFPs is given in Fig. 7(F) as a function of $\gamma_{TPP\text{-}2M}/\gamma_{fit}$. We see that the RMS_i values for IMFPs from both equations show no obvious dependence on either ratio.

4.4 Effect of the bandgap energy on IMFPs from the JTP equation

It has often been difficult to estimate values of E_g when calculating IMFPs for unknown compounds with the TPP-2M equation and this difficulty will continue with use of the JTP equation. We therefore investigated how IMFP values from this equation would change if only rough estimates of E_g could be made. IMFPs were calculated from the JTP equation for three representative compounds (GaAs, E_g = 1.47 eV; Kapton, E_g = 5.4 eV; and LiF, E_g =12.4 eV) with low, medium, and high bandgap energies if E_g was assumed instead to be 0 eV, 2 eV, 4 eV, 5 eV, 6 eV, 8 eV, and 10 eV.

Figures 8(A) to 8(C) show ratios of IMFPs calculated from the JTP equation for the three compounds with the assumed E_g values (lines) to IMFPs calculated from the JTP equation with E_g = 0 eV as a function of electron energy between 50 eV and 200 keV. We see that the IMFP ratios increase with increasing values of E_g. Furthermore, the IMFP ratios for the three compounds are found to be constant with increasing electron energy for energies between 300 eV and 200 keV. However, for energies less than 300 eV, the IMFP ratios increase rapidly with increasing E_g and with decreasing electron energy. This trend is common for all three compounds but is particularly pronounced for Kapton where the IMFP ratio is 1.58 at 54.6 eV and for E_g = 10 eV.

The ratio of the increase in IMFP to the increase in E_g is different for each compound in Figs. 8(A) to 8(C). The IMFP calculated from Eq. (19a) depends inversely on the parameter β which in turn depends on the values of E_p, E_g, and ρ, as shown in Eq. (19b) where E_p is obtained from Eq. (6c). The ratio of the IMFP calculated from the JTP equation for LiF at an energy of 10 keV with E_g = 10 eV to the corresponding IMFP with E_g = 0 is approximately 1.17 while the corresponding ratios are 1.29 for GaAs and 1.30 for Kapton. This result occurs because the value of E_p for LiF (26.0 eV) is larger than those for GaAs (15.6 eV) and Kapton (20.6 eV) while the density of LiF (2.64 g cm^{-3}) is intermediate between those for GaAs (5.32 g cm^{-3}) and Kapton (1.42 g cm^{-3}). The resulting change in β as E_g is varied between 0 and 10 eV is smaller in LiF than those for the other two compounds. That is, the IMFP calculated from the JTP equation for LiF is less sensitive to the value of E_g than for GaAs and Kapton.

The solid circles in Figs. 8(A) to 8(C) show the ratios of IMFPs from the JTP equation with the actual E_g values for GaAs, Kapton, and LiF to those with E_g assumed to be zero as a function of electron energy. It is clear that an E_g value should be chosen as close as possible to the actual value when using the JTP equation to estimate IMFPs for an unknown material.

To investigate further the effect of uncertainty in an assumed E_g value on IMFPs from the JTP equation, we have used this equation to calculate IMFPs for our groups of 45 inorganic compounds and 14 organic compounds with assumed E_g values of 0 eV, 2 eV, 4 eV, 5 eV, 6 eV, 8 eV, and 10 eV. These calculations were made for the same electron energies between 50 eV and 200 keV that were used for the original IMFP calculations for each compound.[13,14] The calculated IMFPs were then compared with the corresponding IMFPs from the JTP equation with the actual E_g values for each compound to obtain values of $< RMS_i >_x$ from Eq. (12) and $\left[RMS_i\right]_x^{max}$ from Eq. (14) for each compound group.

Figure 5(D) shows plots of $< RMS_i >_x$ (solid circles) and $\left[RMS_i\right]_x^{max}$ (solid squares) as a function of the assumed bandgap energy where the red symbols indicate the results for the group of inorganic compounds and the blue symbols show the results for the organic compounds. The solid and dashed lines in Fig. 8(D) are the values of $< RMS_i >_x$ and $\left[RMS_i\right]_x^{max}$, respectively, from Table 4 that were obtained in comparisons of IMFPs from the JTP equation with the actual E_g values for each compound with the corresponding optical IMFPs. The red lines are results for the inorganic compounds and the blue lines are for the organic compounds.

We see that $< RMS_i >_{inorg}$ in Fig. 8(D) is almost constant (about 11.6 %) for E_g values between 0 eV and 6 eV and then increases for larger values of E_g. For $E_g \leq 6$ eV, the resulting $< RMS_i >_{inorg}$ is about 35 % larger than the value of $< RMS_i >_{inorg}$ = 8.5 % from Table 4 that shows results of comparisons of IMFPs from the JTP equation using actual E_g values for each compound with the corresponding optical IMFPs. On the other hand, the value of $\left[RMS_i\right]_{inorg}^{max}$ decreases from 39 % to 32 % as the assumed bandgap energy is increased from 0 eV to 6 eV. The former value is more than 50 % larger than the value $\left[RMS_i\right]_{inorg}^{max}$ = 21.6 % shown in Table 4 that was obtained from comparisons of IMFPs from the JTP equation using actual E_g values with the corresponding optical IMFPs.

These results reflect the distribution of E_g values for our group of inorganic compounds. In other words, the 45 inorganic compounds in our analysis have E_g values over a wide range, from 0 eV to 12.6 eV, and the distribution is not uniform. Nevertheless, we recommend that a bandgap energy of 5 eV be chosen when estimating IMFP values from the JTP equation for an inorganic compound with an unknown bandgap energy. This recommendation is based on the results in Fig. 8(D) that show $< RMS_i >_{inorg}$ is close to its minimum value for E_g = 5 eV and that $\left[RMS_i\right]_{inorg}^{max}$ is also close to its minimum value for E_g = 5 eV.

For organic compounds, the values of $< RMS_i >_{org}$ in Fig. 8(D) for assumed bandgap energies between 0 eV and 6 eV are almost the same as the value (6.8 %) obtained when IMFPs

are calculated with the JTP equation using the actual bandgap energies for this group that range between 4 eV and 6 eV. Furthermore, the values of $\left[RMS_i\right]_{org}^{max}$ in Fig. 8(D) do not vary appreciably with E_g for assumed bandgap energies between 2 eV and 6 eV. In addition, the value of $\left[RMS_i\right]_{org}^{max}$ for an assumed bandgap energy of 4 eV is 16.9 %. This value is only about 20 % larger than the value (14.1 %) found when the IMFPs are calculated from the JTP equation with the actual bandgap energies. This favorable result may occur because the E_g values for our group of 14 organic compounds are uniformly distributed between 0 eV and 8 eV and because their density differences are also relatively small compared to those for the groups of elemental solids and inorganic compounds.

We therefore recommend that E_g be assumed to be 4 eV (for organic compounds) or 5 eV (inorganic compounds) when calculating IMFPs from the JTP equation if the actual value of E_g is unknown. Of course, the actual value of E_g should be utilized if a value can be found.[22, 23,24 , 25,26] Nevertheless, Fig. 8(D) shows that only rough estimates of E_g are needed in many cases. We also suggest that evaluations be made of IMFPs from the JTP equation by varying parameters such as E_g and the density in reasonable ranges for an unknown material.

5. Discussion

We will make comparisons of IMFPs calculated from the JTP equation with IMFPs calculated from other IMFP predictive equations for our groups of elemental solids, inorganic compounds, and organic compounds. We will also make comparisons of predicted IMFPs from the JTP equation with available experimental IMFPs for elemental solids and inorganic compounds. While the JTP equation is an empirical equation, it is based on IMFPs calculated in a consistent way with the full Penn algorithm and the approach of Boutboul *et al.* for nonconductors for 100 materials and for 83 energies between 50 eV and 200 keV. Comparisons have already been made between these IMFPs and available measured IMFPs for some of these materials in our previous papers.[12,13,14] However, experimental IMFPs are available for additional materials (16 elemental solids and 39 inorganic compounds) from elastic-peak electron spectroscopy (EPES) experiments, reflection electron energy-loss spectroscopy (REELS) experiments, and from transmission electron microscopy (TEM) experiments. We will make comparisons between these IMFPs and IMFPs from the JTP equation. We note here that energy-loss functions are not available for these additional materials and it is thus not possible now to calculate IMFPs for them. Nevertheless, these materials can be considered as "test specimens" for assessing the validity and utility of the JTP equation.

5.1 Comparisons of IMFPs from the JTP equation with IMFPs from other predictive

IMFP equations

5.1.1 S1 equation

The S1 predictive IMFP formula was proposed by Seah[27] for electron energies over 100 eV. His equation was derived from our early calculated IMFPs for 41 elemental solids,[28] 15 inorganic compounds,[4] and 14 organic compounds[5] that had been calculated with the non-relativistic Penn algorithm from optical ELFs. The S1 equation can be expressed as follow:

$$\lambda = \frac{\left(4 + 0.44\ Z^{0.5} + 0.104\ \alpha(E) E^{0.872}\right) a^{1.7}}{Z^{0.3}\ (1 - W)} \qquad \text{(nm)}, \qquad (21a)$$

where $\alpha\,(E)$ is the relativistic correction factor given by equation (6b),

$$a = \left(\frac{10^{21} M}{\rho N_A \sum_{i=1}^{n} h_i}\right)^{\frac{1}{3}} \qquad \text{(nm)} \quad , \qquad (21b)$$

N_A is the Avogadro constant, M is the atomic or molecular weight, and h_i is the stoichiometry coefficients for element i in the compound that consisted of n elements. For an elemental solid, h_1 =1 and n = 1. The term Z in Eq. (21a) is the average atomic number for a compound which for a compound consisting of n elements is given by

$$Z = \frac{\sum_{i=1}^{n} h_i Z_i}{\sum_{i=1}^{n} h_i}, \qquad (21c)$$

where Z_i is the atomic number of the constituent element *i.* The term W in Eq. (21a) is the heat of formation for a compound (in eV per atom) which can be empirically related to the bandgap energy:

$$W = 0.02\ E_g. \qquad (21d)$$

We added the relativistic correction term $\alpha\,(E)$ in Eq. (21a) so that the S1 predictive equation could be evaluated for energies up to 200 keV. Seah stated that Eq. (21d) was a correction term for inorganic compounds and was not recommended for use with organic compounds and elemental solids that have bandgaps.[27] However, our comparisons of IMFPs for 14 organic compounds with and without the W term showed that the differences between our optical IMFPs and the calculated IMFPs from the S1 equation were significantly smaller when the W term was included. We therefore included the W term in the S1 equation for all materials with bandgaps.

Table 8 shows the RMS percentage differences, RMS_{total}, from Eq. (10) between IMFPs calculated from the S1 equation (to be referred to as S1 IMFPs) and the optical IMFPs for energies between 100 eV and 200 keV, along with the corresponding results from the JTP equation results for comparison. We also show values of the average of RMS percentage differences, $<RMS_i>_{\text{total}}$, from Eqs. (8) and (12) in similar comparisons. We see that the values of RMS_{total} and $< RMS_i >_{total}$ for the S1 IMFPs are 10.4 % and 8.7 %, respectively. These values are almost the same as the corresponding results for IMFPs from the JTP equation: 10.0 % and 8.4 %, respectively. We give results of similar comparisons in Table 8 for our groups of elemental solids, inorganic compounds, and organic compounds. While the values of RMS_{total} and $< RMS_i >_{total}$ are almost the same for IMFPs from the JTP and S1 equations for the group of elemental solids, the S1 equation gives slightly better results than the JTP equation for the group of inorganic compounds. However, the values of RMS_{org} and $< RMS_i >_{org}$ for IMFPs from the S1 equation for organic compounds are more than twice those for IMFPs from the JTP equation.

5.1.2 TPP-LASSO-S equation

The TPP-LASSO-S predictive IMFP equation was developed by Liu *et al.*[29] using a machine-learning approach to determine suitable descriptors for extending the Bethe equation for inelastic-electron scattering. They utilized the calculated IMFPs of Shinotsuka *et al.*[12,13] for 41 elemental solids and 42 inorganic compounds as reference values and obtained analytical expressions for the parameters β and γ in the Bethe equation in terms of material parameters. The TPP-LASSO-S equation that predicts IMFPs for elemental solids and inorganic compounds for electron energies between 200 eV and 200 keV is:

$$\lambda = \frac{\alpha(E)E}{E_p^2\{\beta \ln[\gamma\alpha(E)E]\}} \quad \text{(nm)}, \tag{22a}$$

where

$$\beta = -0.012 + 0.46\left(\frac{M}{\rho N_\text{v}}\right)^{0.5} - 0.35\left(\frac{M}{\rho N_\text{v}}\right)^{0.4} + 0.019\frac{Z}{N_\text{v}} \quad \left(\text{eV}^{-1}\text{nm}^{-1}\right), \tag{22b}$$

$$\gamma = -0.07 + 0.26\left[\rho\left(E_\text{i} + E_\text{g}\right)\right]^{-0.2} + 0.066\left(\frac{Z\rho}{M}\right)^{-0.8} \quad \left(\text{eV}^{-1}\right), \tag{22c}$$

and where Z is the atomic number or average atomic number for a compound and E_i is the starting point energy that is defined as E_F for elemental solids and as $E_\text{v} + E_\text{g}$ for inorganic compounds.

Table 9 shows the RMS percentage differences, RMS_{total}, from Eq. (10) between IMFPs

calculated from the TPP-LASSO-S equation (to be referred to as LASSO IMFPs) and the optical IMFPs for energies between 200 eV and 200 keV, along with the corresponding results from the JTP equation for comparison. We also show values of the average of RMS percentage differences, $<RMS_i>_{total}$, from Eqs. (8) and (12) in similar comparisons. We see that the values of RMS_{total} and $<RMS_i>_{total}$ for all materials with the LASSO IMFPs are 12.8 % and 10.0 %, respectively. These values are more than 20 % larger than the corresponding values with the JTP equation.

We also give results of similar comparisons in Table 9 for our groups of elemental solids, inorganic compounds, and organic compounds. For the elemental solids, we see that the values of RMS_{elem} from both equations are identical (11.0 %) while the value of $<RMS_i>_{elem}$ from the JTP equation (9.1 %) is slightly larger than the corresponding value from the TPP-LASSO-S equation (8.7 %). For the inorganic compounds, the value of RMS_{inorg} from the JTP equation (9.7 %) is a little smaller than the value from the TPP-LASSO-S equation (11.4 %) while the values of $<RMS_i>_{inorg}$ from both equations are almost the same (8.2 % and 8.4 %, respectively). For the organic compounds, however, the values of RMS_{org} and $<RMS_i>_{org}$ from the TPP-LASSO-S equation (20.1 % and 19.1 %, respectively) are more than twice those from the JTP equation (7.4 % and 6.6 %, respectively). This poor result probably results from the fact that IMFPs for organic compounds were not used in the development of the TPP-LASSO-S equation.

5.1.3 Evaluations of the predictive IMFP equations

Figure 9 shows ratios of IMFPs from the S1 equation (Fig. 9(A)) and from the TPP-LASSO-S equation (Fig. 9(B)) to the optical IMFPs of our 100 materials as a function of electron energy. The lower energy limits in these plots are 100 eV for Fig. 9(A) and 200 eV for Fig. 9(B) since these are the expected lower energy limits for validity of each equation. Figure 9(A) shows that the plotted ratios for IMFPs from the S1 equation are nearly constant for energies between 500 eV and 200 keV. At lower energies, there is more variation of the ratios with energy. The plotted ratios for IMFPs from the TPP-LASSO-S equation in Fig. 9(b) are almost constant for energies above 1000 eV but there are larger variations of the ratios for lower energies. We also note that most of the ratios at an energy of 1 keV are between 0.75 and 1.2 in Fig. 9(A) while most of the ratios are between 0.7 and 1.2 at the same energy in Fig. 9(B). We now examine values of the RMS percentage differences between IMFPs from the JTP, S1, and TPP-LASSO-S equations and the corresponding optical IMFPs, RMS_j, from Eq. (20) as a function of electron energy in Fig. 10. Figure 10(A) shows plots of the RMS_j values found for each equation from IMFPs for our 100 materials. Separate plots are shown for RMS_j values for the groups of elemental solids in Fig. 10(B), inorganic compounds in Fig. 10(C),

and organic compounds in Fig. 10(D).

Figure 10(A) shows that the RMS_j values from the three predictive IMFP equations for our group of materials increase with decreasing energy for energies below 300 eV. Nevertheless, only the JTP equation would be useful for practical applications at energies as low as 50 eV. Although the S1 equation was developed for use at energies above 200 eV, we recommend that its use be restricted to energies above 300 V.

Figures 10(B) and 10(C) show that the RMS_j values for the groups of elemental solids and inorganic compounds from the S1 equation are smaller than those from the JTP equation at energies between 300 eV and 200 keV. However, the RMS_j values from the S1 equation are larger than the RMS_j values from the JTP equation for energies less than 200 eV. For the group of organic compounds, Fig. 10(C) sows that the RMS_j values from the S1 equation are larger than 15 % for energies between 100 eV and 200 keV while RMS_j values from the JTP equation are less than 8 %. The S1 equation is therefore expected to be less reliable than the JTP equation in applications with organic compounds.

Figures 10(B) and 10(C) show that the RMS_j values from the TPP-LASSO-S equation are comparable to those from the JTP equation for energies between 500 eV and 200 keV for our groups of elemental solids and inorganic compounds. For our group of organic compounds, however, Fig. 10(D) shows that the RMS_j values from the TPP-LASSO-S equation are more than twice as large as those from the JTP equation for energies between 200 eV and 200 keV. This result is not surprising since the TPP-LASSO-S equation was not developed for application to organic compounds.[29]

5.2 Comparisons of IMFPs from the JTP equation with measured IMFPs

Figure 11 compares IMFPs calculated from the JTP equation for Zn, Ga, Mn, Te, and Pb with IMFPs from the EPES experiments of Werner *et al.*[30] for energies between 200 eV and 3400 eV, the EPES experiments of Tanuma *et al*.[31] for energies between 50 eV and 5000 eV, the TEM experiments of Iakoubovskii *et al*.[32] at 200 keV, and from the REELS experiments of Werner *et al*.[33] for energies between 100 eV and 10 keV. Figure 11(A) shows the comparisons for Zn. We see that the IMFPs from the JTP equation are in good agreement with the IMFPs of Tanuma *et al.*[31] for energies between 100 eV and 5000 eV, with an RMS difference of 11.4 %. This RMS difference is comparable to the RMS difference of 11.0 % found by Tanuma *et al*.[31] between the IMFPs for 11 elemental solids (graphite, Si, Cr, Fe, Cu, Mo, Ag, Ta, W, Pt and Au) from EPES experiments and the corresponding optical IMFPs. However, for energies between 50 eV and 100 eV, the IMFPs of Tanuma *et al*.[31] show a different dependence on energy from that of the JTP equation. This difference is most likely due to the fact that surface excitations were neglected in the analysis of the EPES results. We

also note that IMFPs from the JTP equation differ from the optical IMFPs for many materials at energies below 100 eV, as shown in Fig. 4(A). Figure 11(A) also shows that the energy dependence of the IMFPs of Werner *et al*.[33] is similar to that of IMFPs from the JTP equation. However, the RMS difference between these IMFPs is relatively large, 18.1 %. We also note that the IMFP from the JTP equation at 200 keV is about 20 % smaller than the IMFP measured by Iakoubovskii *et al*.[32]

Figure 11(B) shows good agreement IMFPs from the JTP equation for Ga with those from the EPES experiments of Tanuma *et al*[31] for energies between 100 eV and 5 keV where the RMS difference of 11.3 %. As for the case of Zn in Fig.11(A), the experimental IMFP for Ga at 50 eV is larger than the value from the JTP equation. The IMFP of Iakoubovskii *et al*. at 200 keV is 17 % smaller than the value from the JTP equation.

Figure 11(C) shows comparisons of IMFPs from the JTP equation for Mn, Te, and Pb with the IMFPs of Werner *et al*.[30] from EPES experiments for energies between 200 eV and 3400 eV and with the IMFPs of Iakoubovskii *et al*. at 200 keV. We also show IMFPs of Te and Pb at energies from 100 eV to 10 keV that were calculated by Werner *et al*.[33] with the Penn algorithm using ELFs obtained from REELS experiments. For Mn, there is good agreement between IMFPs from the JTP equation and the IMFPs from the Werner *et al*. EPES experiments, with an RMS difference of 13.4 %. For Te, the IMFPs from the JTP equation are in excellent agreement with both IMFPs from the EPES experiments and from the REELS experiments, with RMS differences of 7.9 % and 5.4 %, respectively. For Pb, however, the RMS differences between IMFPs from the JTP equation and IMFPs from the Werner *et al*. EPES experiments for energies between 200 eV and 3400 eV and the IMFPs from the Werner *et al*. REELS experiments for energies between 100 eV and 10 keV were 40.5 % and 25.2%, respectively. We also note that the energy dependence of IMFPs from the Werner *et al*. EPES experiments is different from that of IMFPs from the JTP equation. On the other hand, the energy dependence of IMFPs for Pb IMFPs from the REELs experiments of Werner *et al.*[33] is similar to that of the IMFPs from the JTP equation for energies between 100 eV and 10 keV. At 200 keV, the IMFPs of Iakoubovskii *et al*.[32] agree reasonably well with IMFPs from the JTP equation, with differences of 15.7 %, 7.9 %, and 31.4 % for Mn, Te, and Pb, respectively.

Figure 12(A) show IMFPs from the JTP equation versus the corresponding measured IMFPs of Iakoubovskii *et al*.[32] at 200 keV for 16 elemental solids. The solid line indicates perfect correlation between the calculated IMFPs and the measured IMFPs while the dashed lines show IMFP values that are 20 % larger and 20 % smaller than those from the JTP equation. More than 80 % of the plotted points in Fig. 12(A) (13 elemental solids) have differences from the solid line of less than 20 %. However, three solids show differences of more than 20 %: S (-29 %), Tl (48 %), and Pb (31 %). Since there are no details concerning sample preparation

in the Iakoubovskii *et al*. report, [32] we are unable to discuss possible reasons for the larger differences found for S, Tl, and Pb. For the 16 elemental solids, the average RMS difference between the IMFPs from the TEM experiments and those from the JTP equation was 19 %. This average RMS difference is slightly larger than the average RMS differences found in our earlier comparisons of the measured IMFPs of Iakoubovskii *et al*. [32] and the optical IMFPs for 11 elemental solids at 100 keV (18.5 %) and similar comparisons for 32 elemental solids at 200 keV (11.2 %).[12] However, the IMFPs from the JTP equation for more than 80 % of the elemental solids in Fig. 12(A) are within 20 % of the measured IMFPs. If we exclude the measured IMFPs of S, Tl and Pb in the comparisons with IMFPs from the JTP equations, the RMS difference for the other 13 elemental solids decreases to 11.5 %. This RMS difference is then comparable to the RMS difference between the optical IMFPs and the IMFPs for 32 elemental solids from TEM experiments at 200 keV (11.2 %). It is also comparable to the average RMS difference of 11.0 % for 11 elemental solids found previously between the optical IMFPs and EPES IMFPs from EPES experiments for 11 elemental solids for energies between 100 eV and 5000 eV.[31]

Figure 12(B) shows a similar comparison of IMFPs from the JTP equation with the corresponding IMFPs of Iakoubovskii *et al*.[32] from TEM experiments at 200 keV for 37 oxides. For most of these oxides, the measured IMFPs are smaller than the calculated IMFPs. Furthermore, the range of IMFPs from the JTP equation is wider than the range of measured IMFPs. There is one oxide (B_2O_3) that has a calculated IMFP from the JTP equation that is more than 20 % larger than the measured IMFP while there are 17 oxides that have calculated IMFPs more than 20 % smaller than the measured values. The average RMS difference between the IMFPs from the JTP equation and the measured IMFPs for the 37 oxides in Fig. 12(B) is 19.1 %. This value is slightly less than the average RMS difference of 23.5 % between measured IMFPs for seven inorganic compounds and the corresponding optical IMFPs for energies between 24 eV and 300 keV.[13]

We investigated possible correlations between the IMFPs of Iakoubovskii *et al.*[32] from TEM experiments at 200 keV (shown in Figs. 12(A) and (B)) and the four material parameters in the JTP equation (N_v, M, ρ, and E_g). We found that the measured IMFPs showed a weak dependence on bulk density, as shown in Fig. 12(C) for the group of 16 elemental solids and in Fig. 12(D) for the group of 37 inorganic compounds. From Fig. 12(D), we see that the measured IMFPs for the group of inorganic compounds in Fig.12(D) are larger than the IMFPs from the JTP equation for densities larger than about 5 g cm^{-3}. No such trend was found for the group of elemental solids in Fig. 12(C). Since it is challenging to fabricate defect-free and uniform thin films of oxides, it is hard to determine whether the trend shown in Fig. 12(D) is due to possible sample nonuniformities or to limitations of the ρ term in the JTP equation.

To summarize, the average RMS difference between measured IMFPs and IMFPs from the JTP equation is comparable to the RMS differences we have found previously between measured IMFPs and optical IMFPs.[12,13] We therefore believe that IMFPs from the JTP equation should be useful for a wider range of materials than those from the TPP-2M equation.

6. Summary

We calculated IMFPs of Si_3N_4 and LiF for electron energies from 50 eV to 200 keV that were calculated from their optical ELFs using the relativistic FPA including the correction of the bandgap effect in insulators. These calculated IMFPs could be fitted to the relativistic modified Bethe equation for energies between 50 eV and 200 keV. The RMS differences in these fits were less than 1 % for both materials. The IMFPs were also compared with IMFPs from the relativistic TPP-2M equation. We found that IMFPs from the TPP-2M equation were systematically larger than the calculated IMFPs, with RMS differences of 49.3 % for LiF and 17.3 % for Si_3N_4. These RMS differences are much larger than those for most of the inorganic compounds in our previous IMFP calculations for 42 inorganic compounds where the average RMS difference was 10.7 %.

We also reported the development of an improved predictive IMFP equation which we designated as the JTP equation. This equation is a refinement of the TPP-2M equation and is based on recent IMFP calculations with the relativistic FPA for 100 materials including the present IMFPs for Si_3N_4 and LiF for 83 electron energies between 50 eV and 200 keV. The resulting JTP equation gave satisfactory results in comparisons of predicted IMFPs for the 100 materials and the corresponding optical IMFPs. The RMS difference between the 8300 optical IMFPs used for optimization and the IMFPs calculated from the JTP equation was 10.2 %. This value is appreciably less than the RMS difference of 16.0 % found in a similar comparison of the optical IMFPs and IMFPs from the TPP-2M equation.

We also evaluated the JTP equation using values of the RMS percentage difference, RMS_j from Eq. (20), between IMFPs from the JTP equation or the TPP-2M equation and the optical IMFPs at a particular energy for a group of materials (41 elemental solids, 45 inorganic compounds, 14 organic compounds, or all materials). Values of RMS_j for all materials were almost constant for energies between 150 eV and 200 keV with an average value of 10.0 %. At lower energies, RMS_j increased from 10.5 % at 148 eV to 12.4 % at 54 eV. In contrast, values of RMS_j for the TPP-2M equation exceeded 15 % for all energies, with a maximum value of 17.1% at around 90 eV. At higher energies, RMS_j decreased almost uniformly with increasing electron energy and reached a value of 15.4 % at 200 keV.

We also examined how IMFP values from the JTP equation changed if values of the bandgap energy E_g, were not known for a candidate material. For three representative

compounds with low, medium, and high bandgap energies (GaAs, E_g = 1.47 eV; Kapton, E_g = 5.4 eV; and LiF, E_g = 12.4 eV), assumed values of E_g were chosen in 2 eV steps from 0 eV to 10 eV. IMFPs were then calculated from the JTP equation and compared to the IMFPs found with the actual values of E_g for each compound. These comparisons showed that E_g could reasonably be assumed to be 5 eV for an inorganic compound or 4 eV for an organic compound. Of course, the actual value of E_g should be used if it is known. As shown in Fig, 8(d), even a rough estimate of E_g is sufficient for most applications. We also recommend varying parameters in the JTP equation such as the bandgap energy and the density within reasonable ranges to evaluate the likely uncertainty of the calculated IMFP.

We made comparisons of IMFPs calculated from the JTP equation with IMFPs calculated from two other IMFP predictive equations, the Seah S1 equation and the TPP-LASSO-S equation. IMFPs from each equation were calculated for our groups of elemental solids, inorganic compounds, and organic compounds and compared with the optical IMFPs. Values of RMS_j for the JTP equation were constant at about 10 % for energies between 150 eV and 200 keV. These values did not differ significantly among the material groups. While RMS_j values for the Seah S1 equation were comparable to those for the JTP equation for elemental solids and inorganic compounds above 300 eV, the values of RMS_j values for the Seah S1 equation were about 15 % for organic compounds and energies between 100 eV and 200 keV. Values of RMS_j for the TPP-LASSO-S equation were comparable to those from the JTP equation for the group of elemental solids and energies between 200 eV and 200 keV. For the group of inorganic compounds, the RMS_j values for the TPP-LASSO-S equation were between 11 % and 12 % at energies between 500 eV and 200 keV, values that are slightly larger than those from the JTP and S1 equations. On the other hand, the RMS_j values for the group of organic compounds from the TPP-LASSO-S equation were between 19 % and 28 %. These RMS_j values were more than twice as large as those from the JTP equation for energies between 200 eV and 200 keV. This result is not unexpected since the TPP-LASSO-S equation was not developed for application to organic compounds.[29]

We compared IMFPs from the JTP equation with measured IMFPs for 16 elemental solids and 37 inorganic compounds at energies between 50 eV and 200 keV. We note that ELFs are not available for these materials and it is thus not possible to calculate their IMFPs with the Penn algorithm. These materials can then be considered as “test specimens” for assessing the validity and utility of the JTP equation. We found that the RMS difference between the measured IMFPs and the corresponding IMFPs from the JTP equation were comparable to the RMS differences we found previously between measured IMFPs and optical IMFPs.[12,13] We believe that the JTP equation is applicable to a wider range of materials than the TPP-2M equation.

Table 1. Sources of optical data used in the IMFP calculations for LiF and Si_3N_4.

Compound	Photon energy range (eV)	Source of data
LiF	3.718E-08 eV to 30 eV	Refs. 34, 35
	32.5 eV to 1.07 MeV	Ref. 36
Si_3N_4	4.6 eV to 30 eV	Calculation with WIEN2k*
	30.4 eV to 30 keV	Calculation with FEFF*
	30.887 eV to 1 MeV	Ref. 36

* Crystal information used for the optical constant calculations: Space group name: P 63
Cell parameters: a = 7.6316 nm, c = 2.9201 nm, $\gamma = 120^{\circ}$

Table 2. Calculated IMFPs (in nm) for LiF and Si_3N_4 as a function of electron energy *E* with respect to the bottom of the conduction band.

	IMFP (nm)			IMFP (nm)	
E (eV)	LiF	Si_3N_4	*E* (eV)	LiF	Si_3N_4
54.6	0.904	0.555	3641.0	6.86	5.64
60.3	0.830	0.529	4023.9	7.44	6.12
66.7	0.793	0.514	4447.1	8.08	6.65
73.7	0.772	0.508	4914.8	8.77	7.22
81.5	0.761	0.508	5431.7	9.52	7.84
90.0	0.757	0.514	6002.9	10.3	8.52
99.5	0.760	0.524	6634.2	11.2	9.26
109.9	0.768	0.538	7332.0	12.2	10.1
121.5	0.781	0.556	8103.1	13.3	10.9
134.3	0.799	0.577	8955.3	14.4	11.9
148.4	0.820	0.602	9897.1	15.6	12.9
164.0	0.845	0.630	10938	17.0	14.0
181.3	0.874	0.662	12088.4	18.5	15.2
200.3	0.908	0.697	13359.7	20.1	16.6
221.4	0.947	0.737	14764.8	21.8	18.0
244.7	0.991	0.781	16317.6	23.7	19.6
270.4	1.04	0.829	18033.7	25.7	21.2
298.9	1.10	0.881	19930.4	27.9	23.1
330.3	1.16	0.938	22026.5	30.3	25.0
365.0	1.23	0.999	24343.0	32.8	27.2
403.4	1.31	1.07	26903.2	35.6	29.5
445.9	1.40	1.14	29732.6	38.6	31.9
492.7	1.49	1.22	32859.6	41.8	34.6
544.6	1.59	1.30	36315.5	45.2	37.5
601.8	1.71	1.40	40134.8	48.9	40.5
665.1	1.83	1.50	44355.9	52.9	43.8
735.1	1.97	1.61	49020.8	57.2	47.4
812.4	2.12	1.73	54176.4	61.7	51.1
897.8	2.28	1.87	59874.1	66.5	55.1
992.3	2.46	2.01	66171.2	71.6	59.4
1096.6	2.65	2.17	73130.4	77.0	63.9
1212.0	2.86	2.35	80821.6	82.8	68.6
1339.4	3.09	2.53	89321.7	88.8	73.6
1480.3	3.34	2.74	98715.8	95.1	78.9
1636.0	3.61	2.96	109097.8	102	84.4
1808.0	3.90	3.21	120571.7	109	90.1
1998.2	4.23	3.47	133252.4	116	96.0
2208.3	4.58	3.76	147266.6	123	102
2440.6	4.96	4.07	162754.8	131	108
2697.3	5.38	4.42	179871.9	138	115
2981.0	5.83	4.79	198789.2	146	121
3294.5	6.32	5.20			

Table 3. Values of the parameters β, γ, C, D found in the fits of Eq. (6) to the calculated IMFPs for LiF and Si_3N_4 for electron energies between 50 eV and 200 keV in Table 2 and values of *RMS* calculated from Eq. (8).

Compound	β (eV^{-1} nm^{-1})	γ (eV^{-1})	C (nm^{-1})	D (eV nm^{-1})	*RMS* (%)
LiF	0.1337	0.09405	14.58	419.4	0.85
Si_3N_4	0.1817	0.09464	11.61	238.2	0.60

Table 4. Values of parameters describing differences between IMFPs from the JTP equation [Eqs. (6) and (19)] and the calculated optical IMFPs of Shinotsuka *et al.*[12,13,14] and between IMFPs from the TPP-2M equation [Eqs.(6) and (7)] and the optical IMFPs of Shinotsuka *et al*. for energies between 50 eV and 200 keV and between 200 eV and 200 keV. Values are given for the root-mean-square (RMS) percentage difference, RMS_x, from Eq. (10) and for three parameters derived from the average RMS difference between IMFPs from each equation and the optical IMFPs, RMS_i, for 83 electron energies from Eq. (8); the average of the RMS_i values for a material group x that contains m materials, $\langle RMS_i \rangle_x$, from Eq.(12) where the index x represents all materials, elemental solids, inorganic compounds, or organic compounds; the median of the RMS_i values for the material group x, $\left[RMS_i\right]_x^{med}$ from Eq.(13); and the maximum of the RMS_i values for the material group x, $\left[RMS_i\right]_x^{max}$ from Eq. (14). Values are also given for the mean of the absolute percentage differences between IMFPs from each equation and the optical IMFPs, $\langle P_i \rangle_x$, from Eq. (15) for a material group x and the maximum value of P_i, $\left[P_i\right]_x^{max}$, from Eq. (18) for the material group x. All values are percentages.

All materials (m = 100)	JTP Equation		TPP-2M Equation	
Energy range	50 eV to 200 keV	200 eV to 200 keV	50 eV to 200 keV	200 eV to 200 keV
RMS_{total}	10.2	10.0	16.0	15.8
$< RMS_i >_{total}$	8.7	8.3	11.1	10.6
$\left[RMS_i\right]_{total}^{med}$	7.3	6.7	8.3	7.7
$\left[RMS_i\right]_{total}^{max}$	23.7	21.7	70.6	71.5
$< P_i >_{total}$	8.1	8.1	10.5	10.3
$\left[P_i\right]_{total}^{max}$	36.0	27.9	75.0	74.2
Elemental solids (m = 41)				
RMS_{elem}	11.1	11.0	17.5	17.3
$< RMS_i >_{elem}$	9.6	9.1	11.9	11.3
$\left[RMS_i\right]_{elem}^{med}$	8.0	6.7	8.2	7.6
$\left[RMS_i\right]_{elem}^{max}$	23.7	21.7	70.6	71.5
$< P_i >_{elem}$	8.8	8.8	11.2	11.1
$\left[P_i\right]_{elem}^{max}$	36.0	27.9	75.0	74.2
Inorganic compounds (m = 45)				
RMS_{inorg}	10.0	9.7	16.5	16.4
$< RMS_i >_{inorg}$	8.5	8.1	11.6	11.2
$\left[RMS_i\right]_{inorg}^{med}$	7.2	6.1	8.9	9.0
$\left[RMS_i\right]_{inorg}^{max}$	21.6	21.2	65.6	66.1
$< P_i >_{inorg}$	8.1	8.0	11.0	10.9
$\left[P_i\right]_{inorg}^{max}$	35.0	25.4	74.4	72.2
Organic compounds (m =14)				
RMS_{org}	7.6	7.4	7.9	7.3
$< RMS_i >_{org}$	6.8	6.6	7.1	6.2
$\left[RMS_i\right]_{org}^{med}$	6.7	6.9	7.7	7.1
$\left[RMS_i\right]_{org}^{max}$	14.1	13.0	13.0	11.5
$< P_i >_{org}$	6.5	6.2	6.6	6.2
$\left[P_i\right]_{org}^{max}$	21.4	16.6	28.9	13.7

Table 5. Values of RMS_i and $[P_i]^{max}$ that describe differences between IMFPs from the JTP equation [Eqs. (6) and (19)] and the calculated optical IMFPs of Shinotsuka *et al*.[12,13,14] and between IMFPs from the TPP-2M equation [Eqs. (6) and (7)] and the optical IMFPs of Shinotsuka *et al*. for the 41 elemental solids and energies between 50 eV and 200 keV. RMS_i is the root-mean-square percentage difference from Equation (8) and $[P_i]^{max}$ is the maximum absolute percentage difference for material *i* from Equation (17).

	RMS_i (%)		$[P_i]^{max}$ (%)	
Material	**JTP equation**	**TPP-2M equation**	**JTP equation**	**TPP-2M equation**
Li	14.2	15.4	19.7	17.5
Be	18.1	22.5	36	29.7
Graphite	23.7	46.6	35.3	54.8
Diamond	21.9	70.6	31.1	75.0
Glassy carbon	11.5	1.8	14.5	2.6
Na	6.9	3.8	11	5.7
Mg	5.3	8.5	14.2	10.2
Al	7.0	10.3	24.9	19.7
Si	8.1	3.7	10.9	4.8
K	16.3	2.9	21	11.2
Sc	18.3	24.2	21.9	26.6
Ti	13.6	19.3	16.9	22.3
V	3.3	7.2	8.7	8.9
Cr	2.8	4.1	4.4	5.9
Fe	11.5	3.8	13.1	6.6
Co	5.3	6.7	10.7	21.3
Ni	8.7	7.4	12.3	26.5
Cu	18.0	12.2	20.9	30.3
Ge	2.2	4.6	11.3	14.3
Y	6.7	13.2	9.5	16.0
Nb	7.4	4.9	22.4	16.8
Mo	5.3	5.2	9.1	8.7
Ru	4.6	3.8	6.4	11.1
Rh	6.2	5.6	8.3	12.0
Pd	3.5	4.6	5.6	15.3
Ag	8.0	9.0	23.8	29.7
In	13.9	19.4	16.4	22.3
Sn	8.6	5.6	21.5	15.1
Cs	9.4	34.7	26	43.5
Gd	8.0	6.9	10.8	10.9
Tb	6.0	8.9	7.9	13.4
Dy	2.0	3.1	6.2	5.1
Hf	12.3	11.8	14.4	14.0
Ta	18.7	15.0	21.9	25.8
W	14.4	7.0	17.2	15.3
Re	14.4	4.4	17.2	8.2
Os	5.6	8.2	9.4	12.7
Ir	5.0	8.3	6.1	11.3
Pt	2.2	10.7	5.1	12.5
Au	3.6	11.3	11.1	17.1
Bi	9.3	12.5	11.1	14.3

Table 6. Values of RMS_i and $[P_i]^{max}$ that describe differences between IMFPs from the JTP equation [Eqs. (6) and (19)] and the calculated optical IMFPs of Shinotsuka *et al.*[12-14] and between IMFPs from the TPP-2M equation [Eqs. (6) and (7)] and the optical IMFPs of Shinotsuka *et al*. for the 45 inorganic compounds and energies between 50 eV and 200 keV. RMS_i is the root-mean-square percentage difference from Equation (8) and $[P_i]^{max}$ is the maximum absolute percentage difference for material *i* from Equation (17).

	RMS_i (%)		$[P_i]^{max}$ (%)	
Material	**JTP**	**TPP-2M**	**JTP**	**TPP-2M**
AgBr	14.0	9.2	15.4	11.1
AgCl	15.1	8.1	16.9	13.9
h-AgI	13.3	9.1	16.3	10.6
Al_2O_3	6.9	17.1	15.4	19.0
AlAs	5.2	3.2	13.3	12.3
h-AlN	1.2	13.9	3.6	16.5
AlSb	2.9	4.5	11.4	12.3
c-BN	19.1	65.6	29.0	74.4
h-BN	12.0	34.3	21.4	44.1
h-CdS	16.6	9.9	19.2	12.2
h-CdSe	16.4	11.6	18.6	13.8
CdTe	11.8	7.7	16.5	10.9
GaAs	2.0	5.0	10.2	13.3
h-GaN	5.3	3.4	12.9	10.1
GaP	3.1	4.3	11.0	11.7
GaSb	4.3	9.0	9.7	14.0
h-GaSe	3.9	2.4	6.6	9.1
InAs	4.1	8.9	5.9	10.4
InP	2.3	6.6	4.4	8.9
InSb	7.8	13.4	11.1	16.8
KBr	11.3	8.1	28.0	30.5
KCl	8.9	6.8	24.0	29.5
LiF	8.2	49.3	11.4	61.7
MgF_2	10.6	19.3	28.6	23.2
MgO	8.3	9.4	18.4	12.8
NaCl	21.6	17.5	24.4	26.9
$NbC_{0.712}$	3.8	2.5	5.8	5.5
$NbC_{0.844}$	4.4	2.6	6.6	5.1
$NbC_{0.93}$	4.9	2.8	7.1	4.8
PbS	3.1	6.6	5.2	10.8
PbSe	5.9	9.6	7.5	16.7
PbTe	11.0	15.4	14.0	21.1
Si_3N_4	1.2	17.3	3.2	18.8
SiC	5.0	16.3	13.8	25.0
SiO_2	12.3	3.0	15.7	11.5
SnTe	7.2	11.6	10.1	15.3
$TiC_{0.7}$	5.9	13.2	8.0	15.5
$TiC_{0.95}$	7.4	16.2	9.8	18.8

$VC_{0.76}$	5.5	3.7	7.9	6.0
$VC_{0.86}$	4.2	5.4	6.4	7.7
Water	4.3	8.3	7.7	7.7
$Y_3Al_5O_{12}$	14.6	7.2	35.0	32.0
ZnS	15.7	5.7	18.6	15.0
ZnSe	17.3	10.8	19.7	12.6
ZnTe	13.1	8.2	16.9	11.1

Table 7. Values of RMS_i and $\left[P_i\right]^{max}$ that describe differences between IMFPs from the JTP equation [Eqs. (6) and (19)] and the calculated optical IMFPs of Shinotsuka *et al.*[12-14] and between IMFPs from the TPP-2M equation [Eqs. (6) and (7)] and the optical IMFPs of Shinotsuka *et al*. for the 14 organic compounds and energies between 50 eV and 200 keV. RMS_i is the root-mean-square percentage difference from Equation (8) and $\left[P_i\right]^{max}$ is the maximum absolute percentage difference for material *i* from Equation (17).

	RMS_i (%)		$[P_i]^{max}$ (%)	
Material	**JTP**	**TPP-2M**	**JTP**	**TPP-2M**
26-n-paraffin	4.8	1.9	13.8	12.6
Adenine	4.1	1.8	6.5	11.5
β-Carotene	6.9	11.4	9.4	26.0
Diphenyl-hexatriene	8.2	13.0	10.4	28.9
Guanine	2.3	9.2	4.3	10.2
Kapton	7.5	4.8	12.9	22.9
Polyacetylene	11.4	10.1	14.5	10.9
Poly(butene-1-sulfone)	6.4	2.7	8.1	14.7
Polyethylene	14.1	7.1	21.4	10.2
Polymethylmethacrylate	11.0	10.1	12.9	24.0
Polystyrene	5.5	8.7	7.6	24.1
Poly(2-vinylpridine)	7.3	8.3	9.5	23.1
Thymine	2.8	4.2	4.6	8.2
Uracil	2.9	6.5	8.7	7.1

Table 8. Values of the RMS percentage difference, RMS_{total}, from Eq. (10) and the average of the RMS percentage differences, $\langle RMS_i \rangle_{total}$, from Eqs. (8) and (12) in comparisons of IMFPs from the JTP equation [Eqs. (6) and (19)] and from the S1 equation [Eq. (21)] with the calculated optical IMFPs of Shinotsuka *et al*.[12-14] for energies between 100 eV and 200 keV. Values are also shown for RMS_x from Eq. (10) and $\langle RMS_i \rangle_x$ from Eqs. (8) and (12) in similar comparisons for a material group *x*.

All materials (m = 100)	JTP Equation	S1 Equation
Energy range	100 eV to 200 keV	100 eV to 200 keV
RMS_{total}	10.0	10.4
$< RMS_i >_{total}$	8.4	8.7
Elemental solids (m = 41)		
RMS_{elem}	11.0	10.0
$< RMS_i >_{elem}$	9.3	8.7
Inorganic compounds (m = 45)		
RMS_{inorg}	9.8	8.2
$< RMS_i >_{inorg}$	8.3	6.6
Organic compounds (m =14)		
RMS_{org}	7.5	16.3
$< RMS_i >_{org}$	6.6	15.2

Table 9. Values of the RMS percentage difference, RMS_{total}, from Eq. (10) and the average of the RMS percentage differences, $\langle RMS_i \rangle_{total}$, from Eqs. (8) and (12) in comparisons of IMFPs from the JTP equation [Eqs. (6) and (19)] and from the TPP-LASSO-S equation [Eq. (21)] with the calculated optical IMFPs of Shinotsuka *et al*.[12-14] for energies between 200 eV and 200 keV. Values are also shown for RMS_x from Eq. (10) and $\langle RMS_i \rangle_x$ from Eqs. (8) and (12) in similar comparisons for a material group *x*.

All materials (m = 100)	JTP Equation	TPP-LASSO-S Equation
Energy range	200 eV to 200 keV	200 eV to 200 keV
RMS_{total}	10.0	12.8
$\langle RMS_i \rangle_{total}$	8.3	10.0
Elemental solids (m = 41)		
RMS_{elem}	11.0	11.0
$\langle RMS_i \rangle_{elem}$	9.1	8.7
Inorganic compounds (m = 45)		
RMS_{inorg}	9.7	11.4
$\langle RMS_i \rangle_{inorg}$	8.2	8.4
Organic compounds (m =14)		
RMS_{org}	7.4	20.1
$\langle RMS_i \rangle_{org}$	6.6	19.1

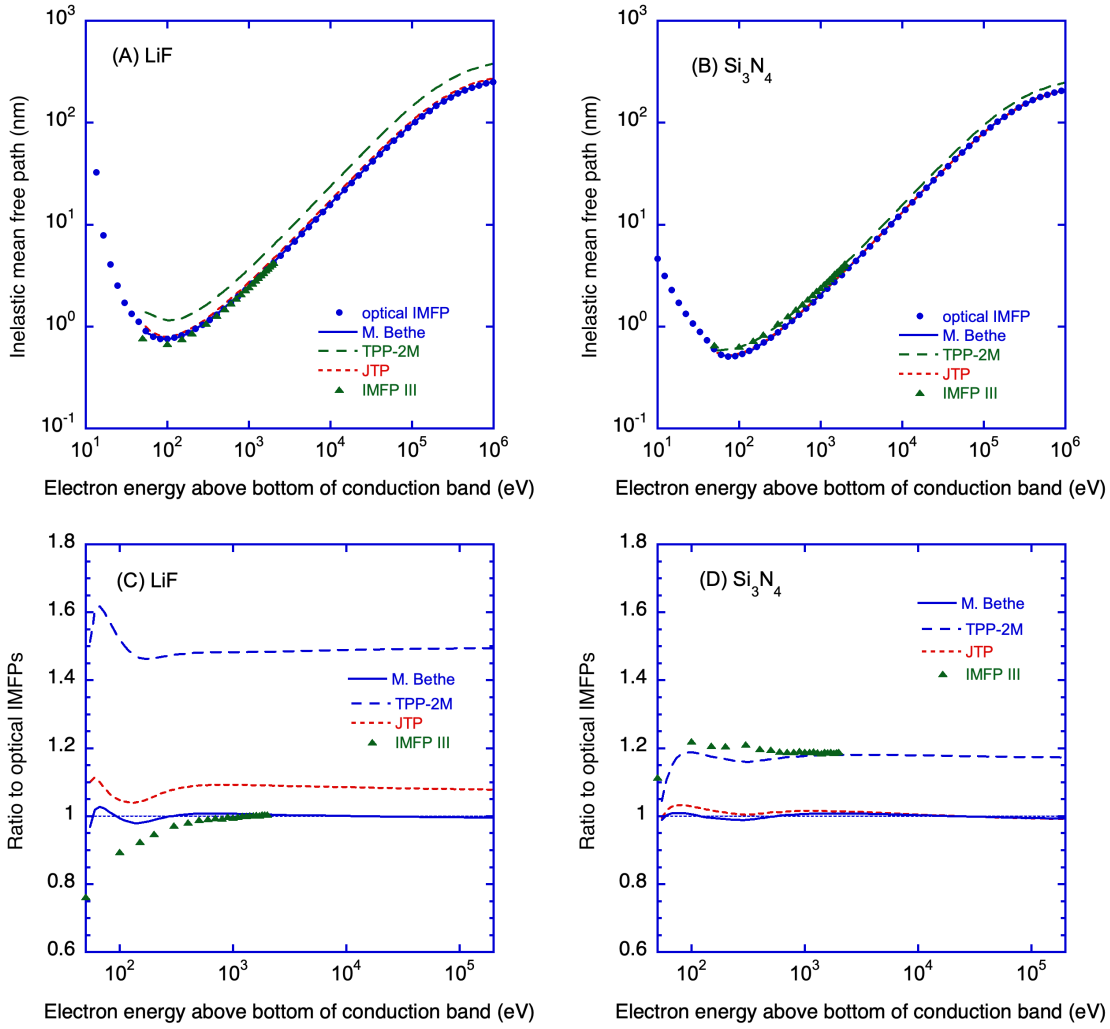

Figure 1. Plots of the calculated inelastic mean free paths (solid circles) as a function of electron kinetic energy above the bottom of the conduction band for (A) LiF and (B) Si_3N_4. The triangles show the previously published IMFPs of Tanuma *et al.*[4] The solid lines show fits to the new IMFPs with the relativistic modified Bethe (M. Bethe) equation [Eq. (6)]. The long-dashed lines indicate IMFPs calculated from the relativistic TPP-2M equation [Eqs. (6) and (7)]. The dotted lines indicate IMFPs calculated from the JTP equation [Eqs.(6) and 19)]. (C) and (D) Plots of ratios of IMFPs from the M. Bethe equation, from the TPP-2M equation, from the JTP equation, and from Tanuma *et al.*[4] to the new IMFPs as a function of electron kinetic energy for (C) LiF and (D) Si_3N_4.

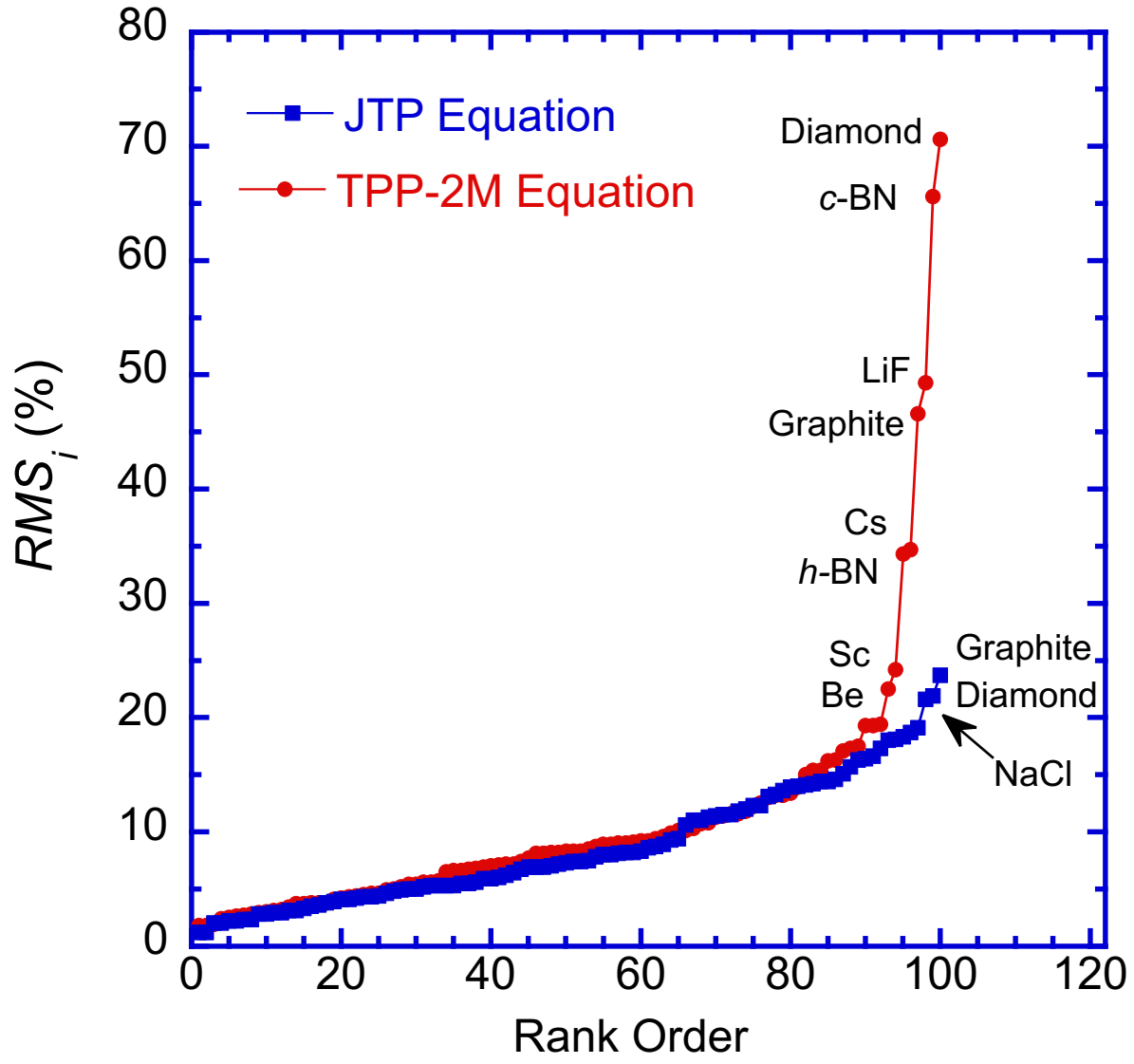

Figure 2. Rank order diagram for the values of RMS_i from Eq. (8) for the 100 materials. Values of RMS_i were evaluated for IMFPs from the TPP-2M equation (solid circles) and from the JTP equation described in Section 4 (solid squares).

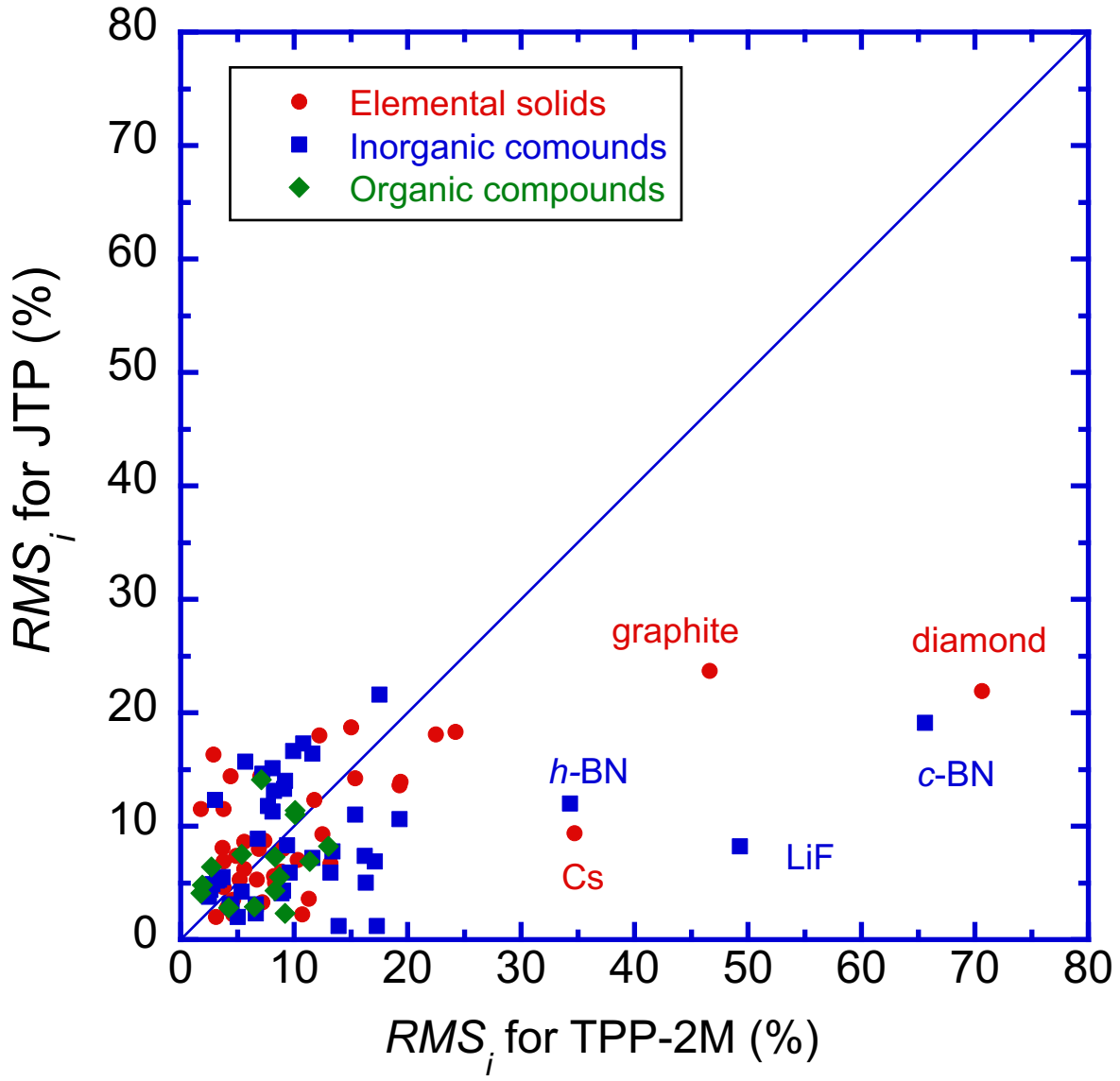

Figure 3. Values of RMS_i obtained from Eq.(8) with IMFPs calculated from the JTP equation (Eqs. 6 and 19) *vs.* the corresponding values of RMS_i with IMFPs calculated from the TPP-2M equation (Eqs. 6 and 7). Solid circles: elemental solids; Solid squares: inorganic compounds; Solid diamonds: organic compounds.

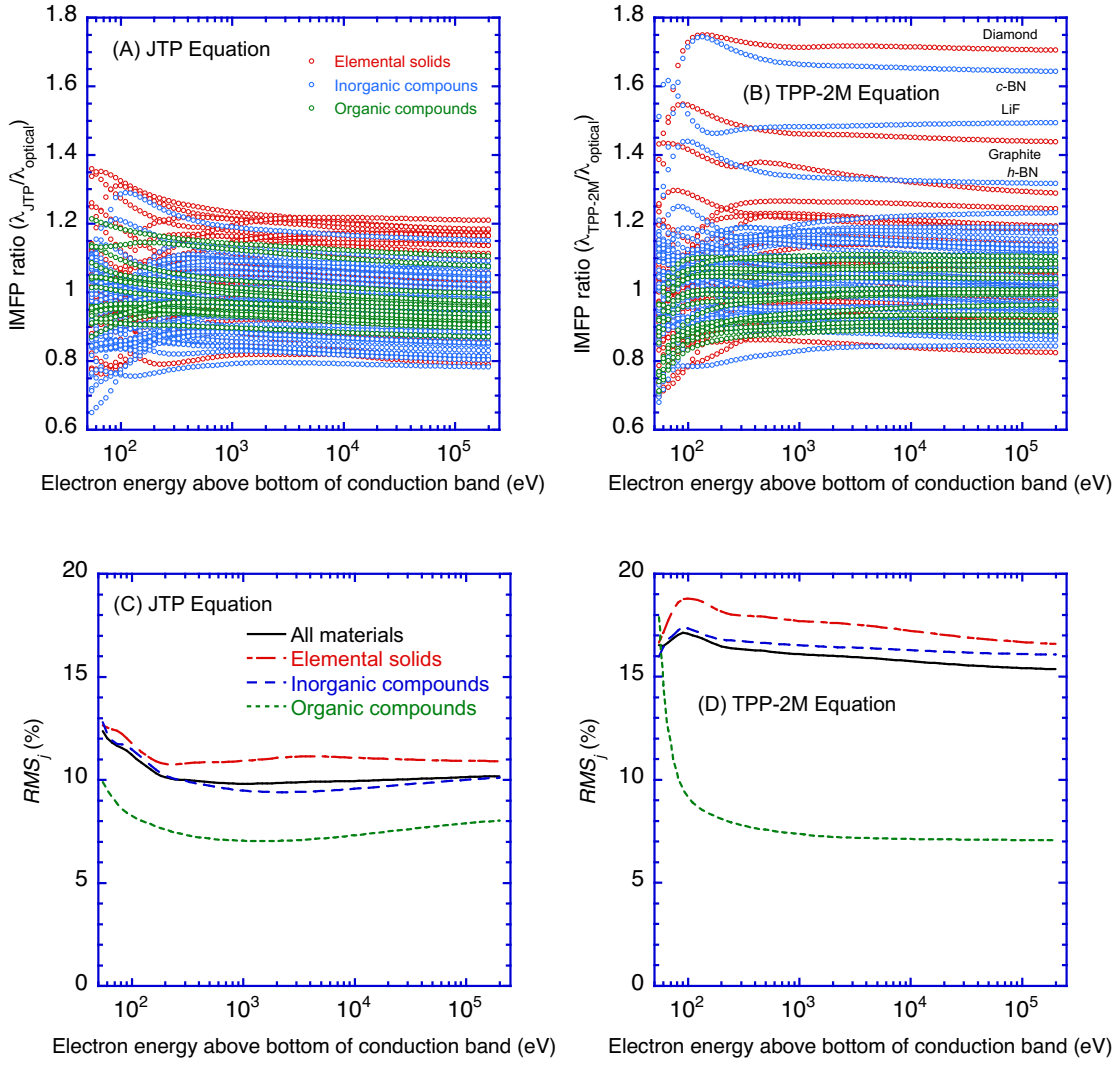

Fig. 4. (A, B) Ratios of IMFPs calculated from the JTP equation (Eqs. 6 and 19) (A) and from the TPP-2M equation (Eqs. 6 and 7) (B) to IMFPs calculated from optical data with the relativistic full Penn algorithm[12] and the Boutboul *et al.*[17] approach for nonconductors as a function of electron energy for 41 elemental solids, 45 inorganic compounds, and 14 organic compounds. (C, D) Values of RMS_j (Eq. 20) plotted as a function of electronic energy for all materials, elemental solids, inorganic compounds, and organic compounds for IMFPs obtained from the JTP equation (C) and the TPP-2M equation (D).

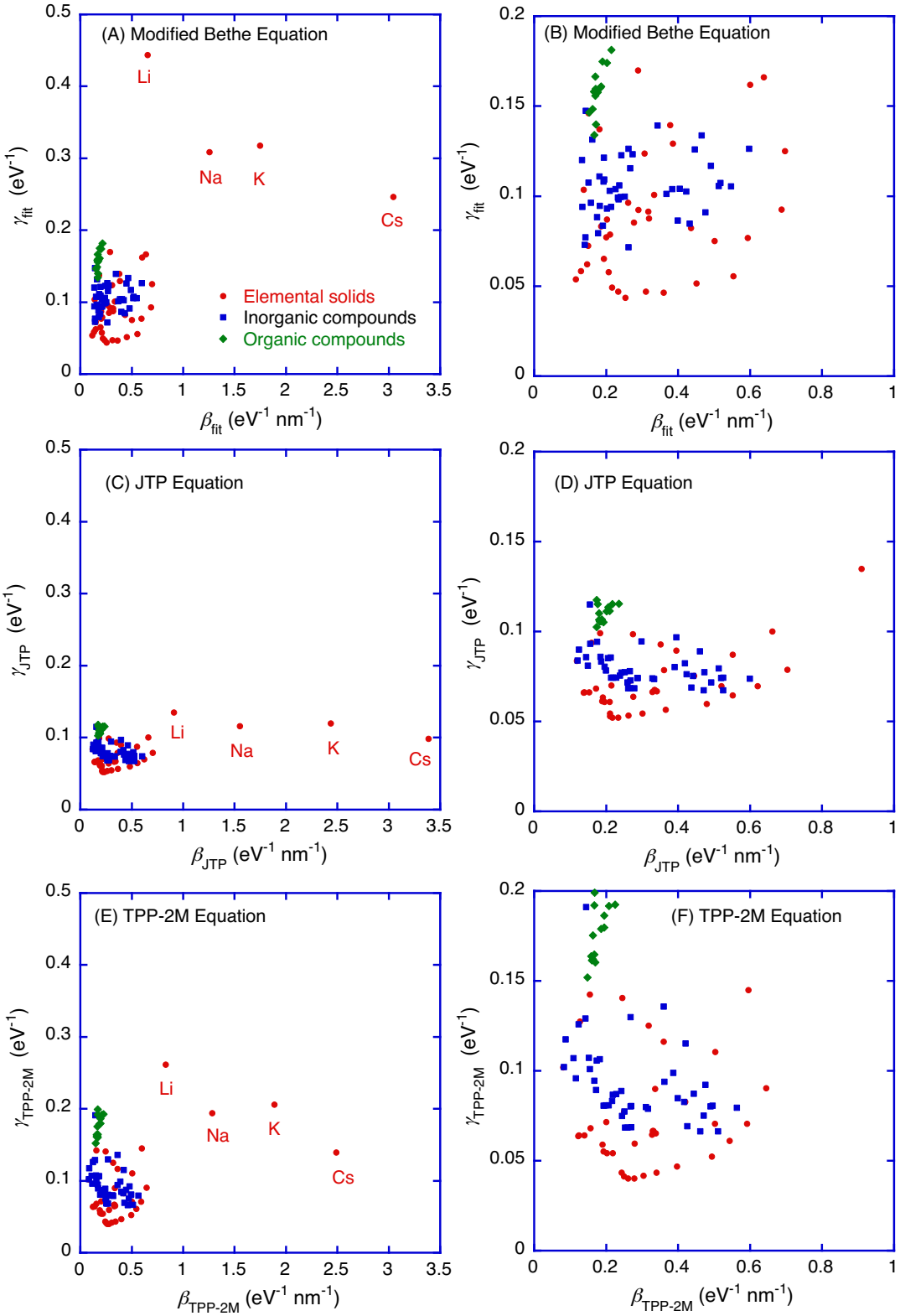

Figure 5. Plots of γ versus β for our 100 materials obtained from (A and B) the modified

Bethe equation, (C and D) the JTP equation, and (E and F) the TPP-2M equation. Solid circles indicate results for elemental solids, solid squares for inorganic compounds, and solid diamonds for organic compounds.

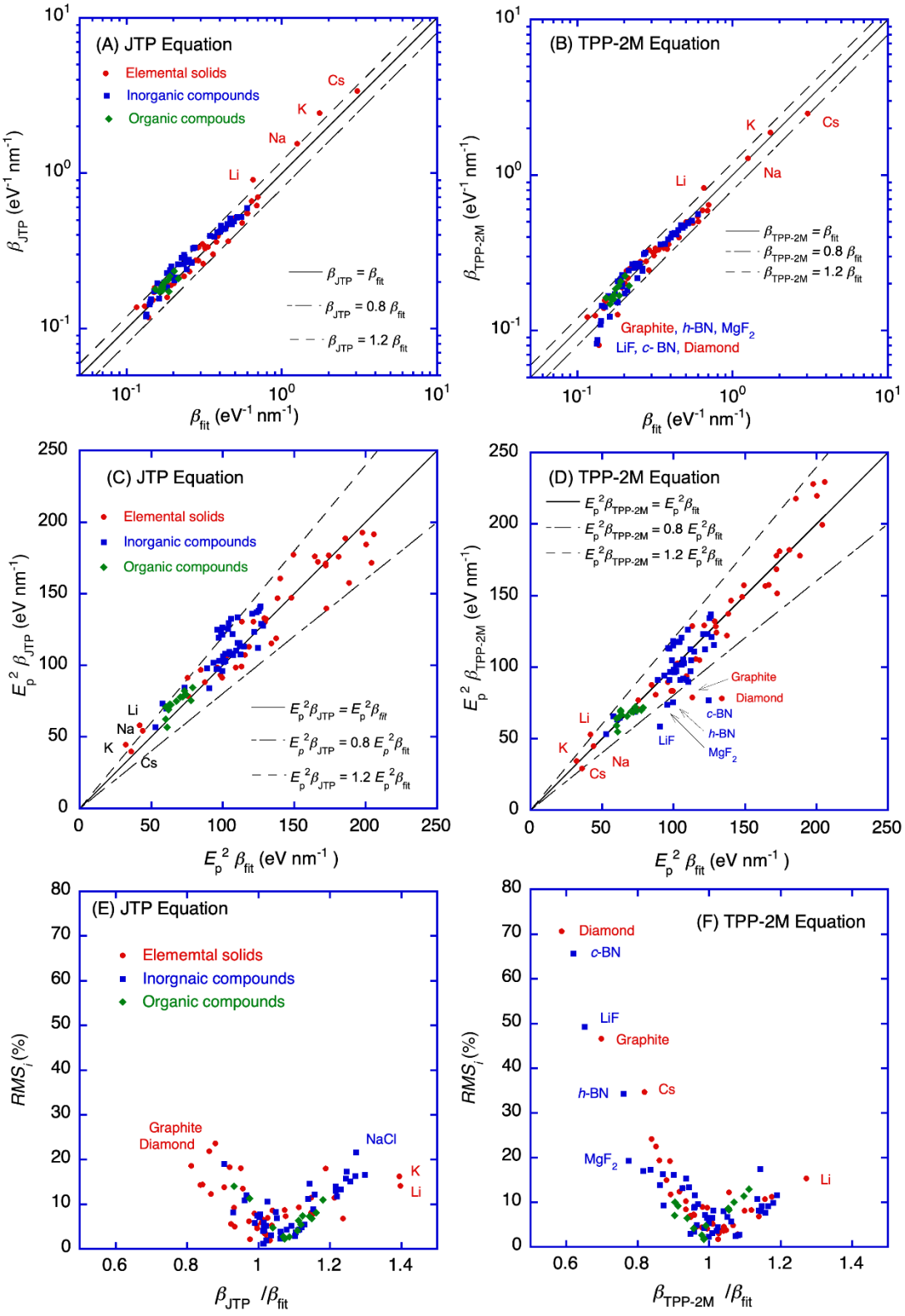

Figure 6. (A) Plot of β_{JTP} (symbols) from Eq. 7(a) for our 100 materials as a function of the corresponding values of β_{fit}. (B) Plot of $\beta_{TPP\text{-}2M}$ (symbols) from Eq. 19(b) as a function of β_{fit}. (C) Plot of $E_p^2\beta_{JTP}$ (symbols) for our 100 materials as a function of the corresponding values of $E_p^2\beta_{fit}$. (D) Plot of $E_p^2\beta_{TPP\text{-}2M}$ (symbols) as a function of $E_p^2\beta_{fit}$.
The solid lines in (A),(B), (C), and (D) indicate perfect correlation between the β or $E_p^2\beta$ values from each equation and β_{fit} or $E_p^2\beta_{fit}$ while the dashed lines indicate β or $E_p^2\beta$ values that are 20 % larger or smaller than the values for the solid line. (E) Plot of RMS_i values for IMFPs from the JTP equation as a function of β_{JTP}/β_{fit}. (F) Plot of RMS_i values for IMFPs from the TPP-2M equation as a function of $\beta_{TPP\text{-}2M}/\beta_{fit}$.

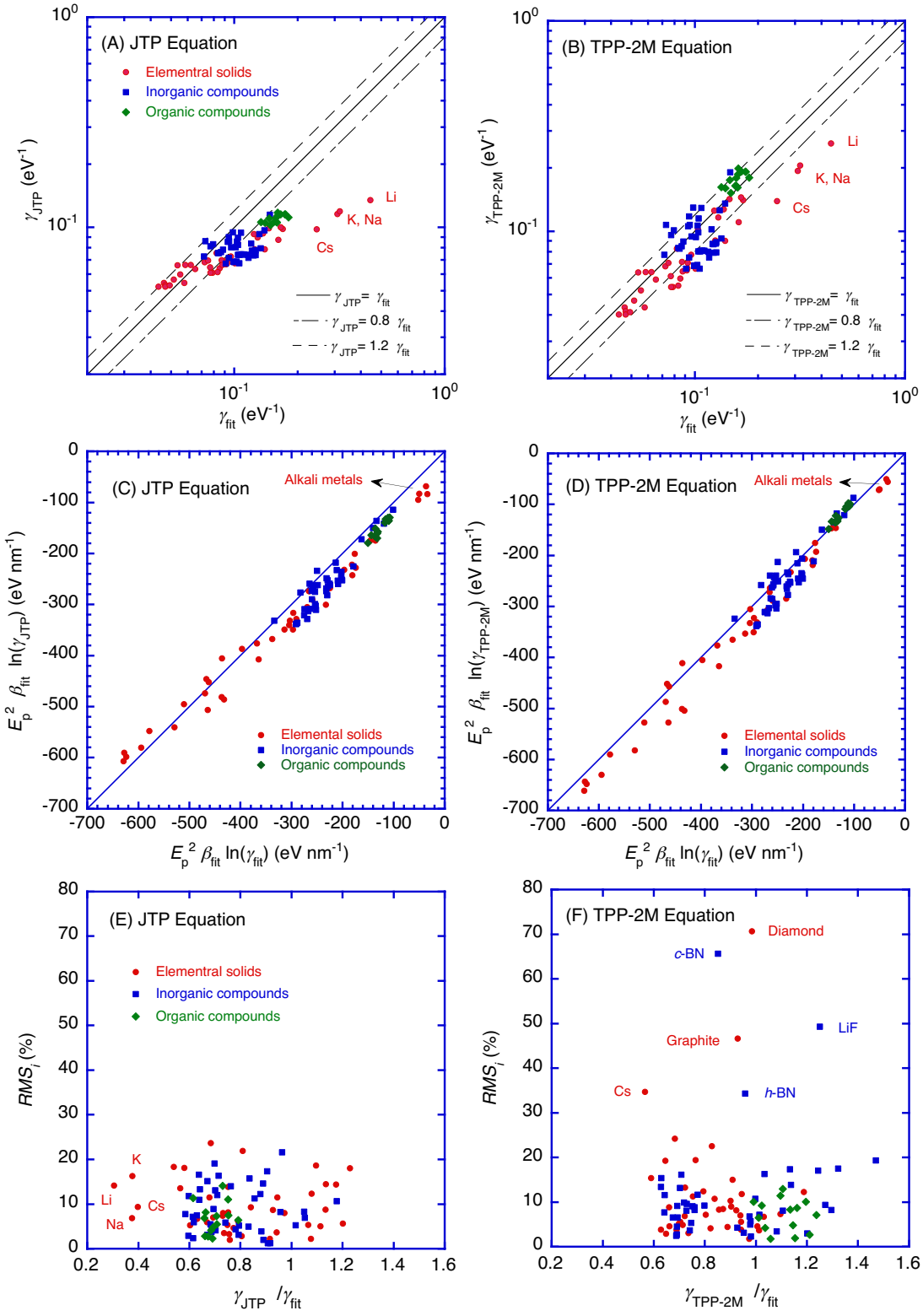

Figure 7. (A) Plot of γ_{TP} from Eq. (7b) for our 100 materials (symbols) as a function of the

corresponding values of $\gamma_{\rm fit}$. (B) Plot of $\gamma_{\rm TPP\text{-}2M}$ from Eq. (19(c)) (symbols) as a function of $\gamma_{\rm fit}$. The solid lines in (A) and (B) indicate perfect correlation between the γ values from each equation and $\gamma_{\rm fit}$ while the dashed lines indicate γ values that are 20 % larger or smaller than the values for the solid line. (C) Plot of $E_{\rm p}^2\beta_{\rm fit}$ ln($\gamma_{\rm TP}$) (symbols) for our 100 materials as a function of the corresponding values of $E_{\rm p}^2\beta_{\rm fit}$ln($\gamma_{\rm fit}$) with $\gamma_{\rm fit}$ expressed in $\rm eV^{-1}$. (D) Plot of $E_{\rm p}^2\beta_{\rm fit}$ ln($\gamma_{\rm TPP\text{-}2M}$) (symbols) for our 100 materials as a function of the corresponding values of $E_{\rm p}^2\beta_{\rm fit}$ln($\gamma_{\rm fit}$) with $\gamma_{\rm fit}$ expressed in $\rm eV^{-1}$. (E) Plot of RMS_i values for IMFPs from the JTP equation as a function of $\gamma_{\rm TP}/\gamma_{\rm fit}$. (F) Plot of RMS_i values for IMFPs from the TPP-2M equation as a function of $\gamma_{\rm TPP\text{-}2M}/\gamma_{\rm fit}$.

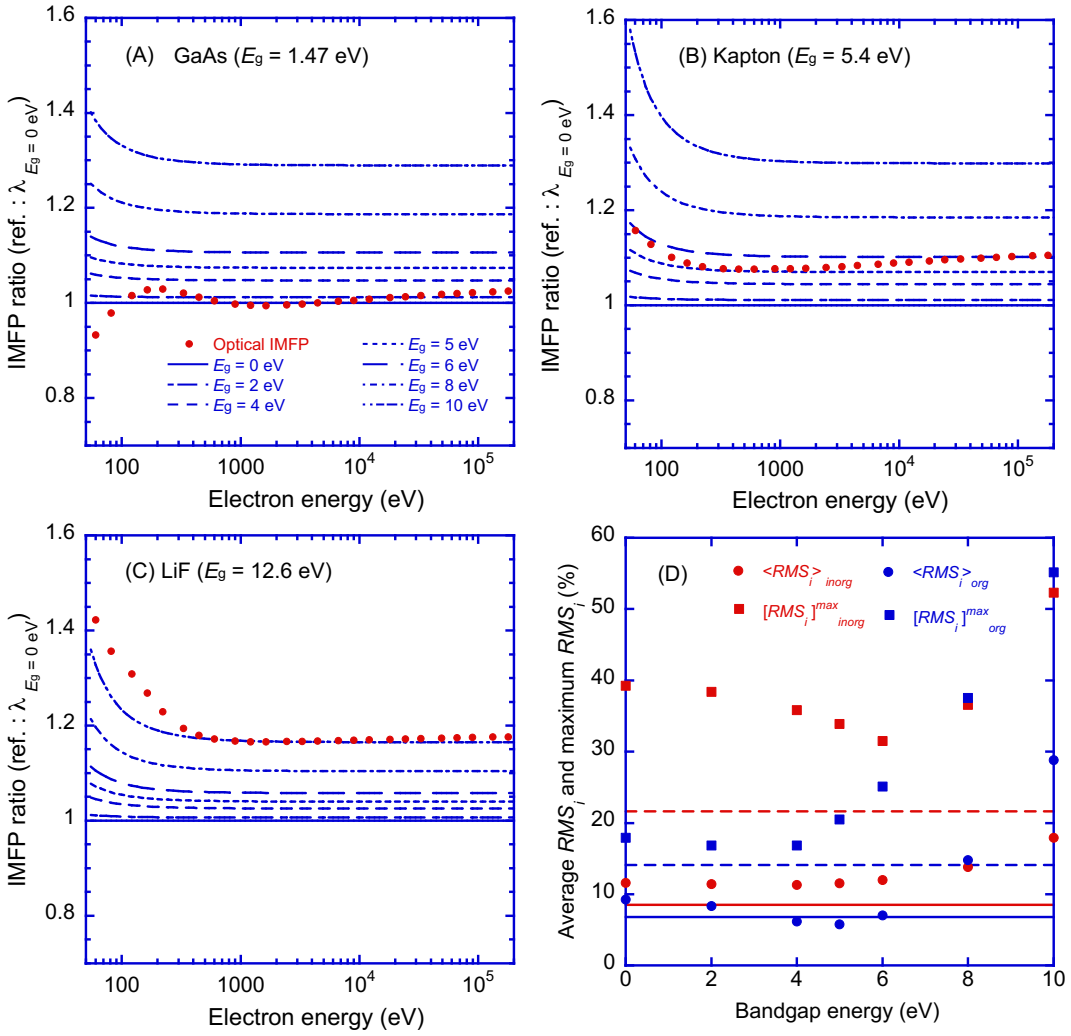

Figure 8. (A, B, C) Ratios of IMFPs calculated from the JTP equation for (A) GaAs, (B) Kapton, and (C) LiF with assumed values of the bandgap energy of 0 eV, 2 eV, 4 eV, 5 eV, 6 eV, 8 eV, and 10 eV (lines) to IMFPs calculated from the JTP equation with E_g = 0 eV as a function of electron energy between 50 eV and 200 keV. The solid circles in Figs. 5(A) to 5(C) show the ratios of IMFPs from the JTP equation with the actual E_g values for GaAs, Kapton, and LiF to those with E_g assumed to be zero as a function of electron energy. (D) Plots of $<RMS_i>$ (solid circles) from Eq. (12) and $[RMS_i]_x^{max}$ (solid squares) from Eq. (14) as a function of the assumed bandgap energy where the red symbols indicate results for the group of inorganic compounds and the blue symbols show the results for the organic compounds. The comparisons were made between IMFPs from the JTP equation and the optical IMFPs. The solid and dashed lines are

the values of $\langle RMS_i \rangle$ and $[RMS_i]_x^{max,}$ respectively, from Table 4 that were obtained in comparisons of IMFPs from the JTP equation with the actual E_g values for each compound with the optical IMFPs for compound. The red lines are results for the inorganic compounds and the blue lines are for the organic compounds.

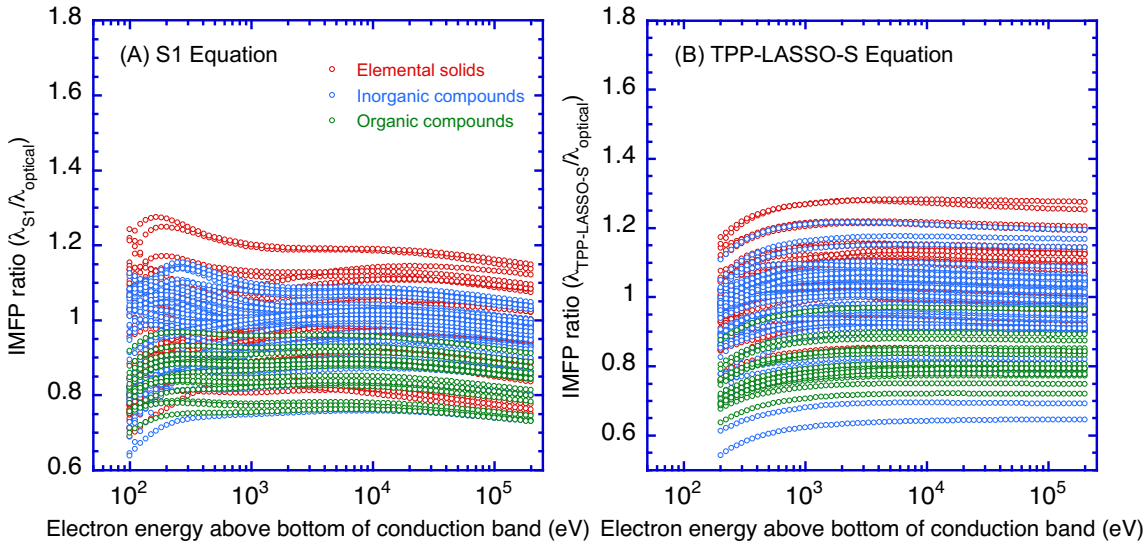

Figure 9. (A) Ratios of IMFPs from the S1 equation (Equation 21) to IMFPs calculated from optical data as a function of electron energy for our groups of 41 elemental solids, 45 inorganic compounds, and 14 organic compounds. (B) Ratios of IMFPs from the TPP-LASSO-S equation (Eq. 22) to IMFPs calculated from optical data as a function of electron energy for our groups of 41 elemental solids, 45 inorganic compounds, and 14 organic compounds.

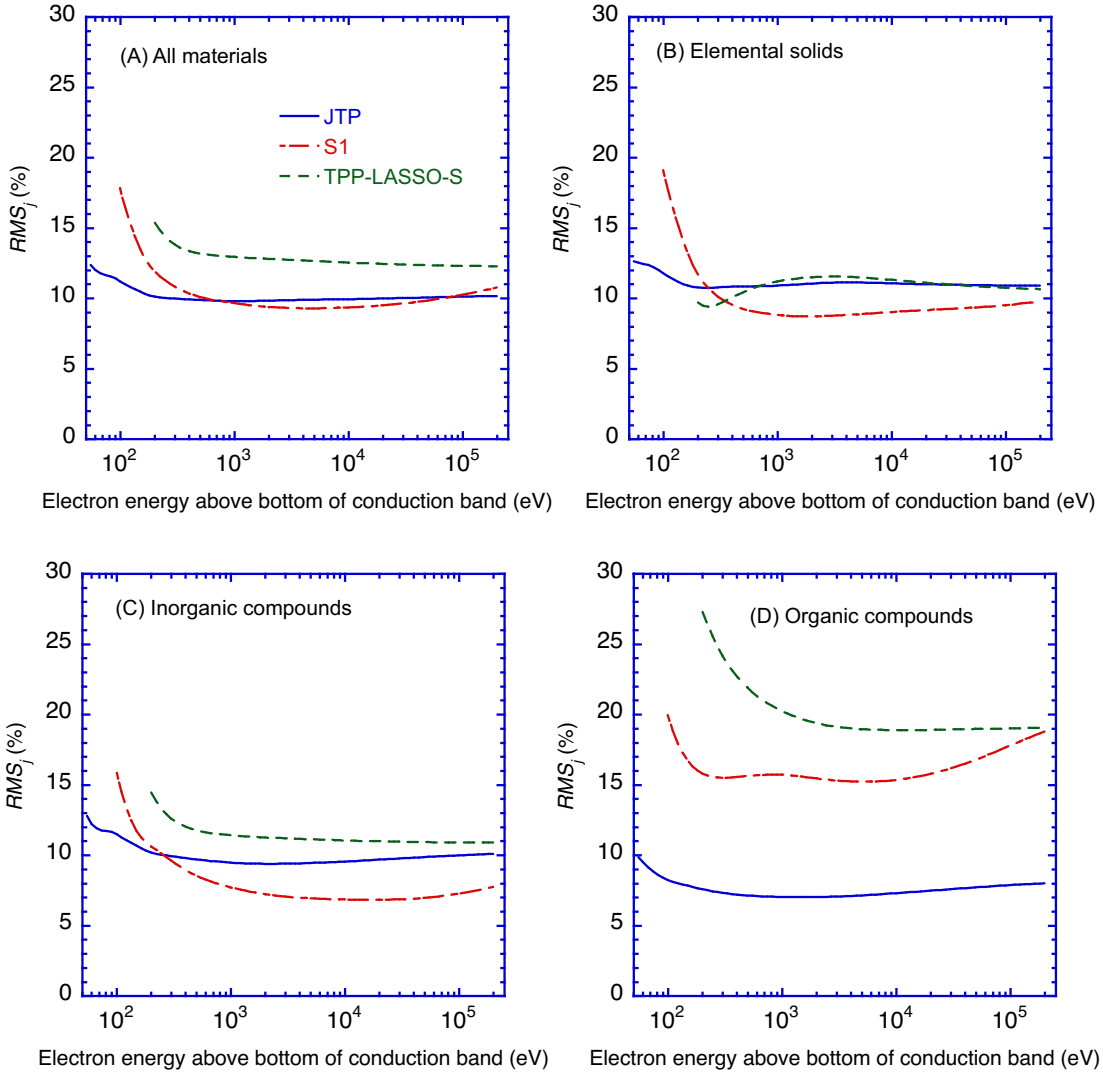

Fig. 10. Plots of RMS_j (Eq. 20) for (A) all materials, (B) elemental solids, (C) inorganic compounds, and (D) organic compounds given by the JTP, S1, and TPP-LASSO-S equations as a function of electron energy.

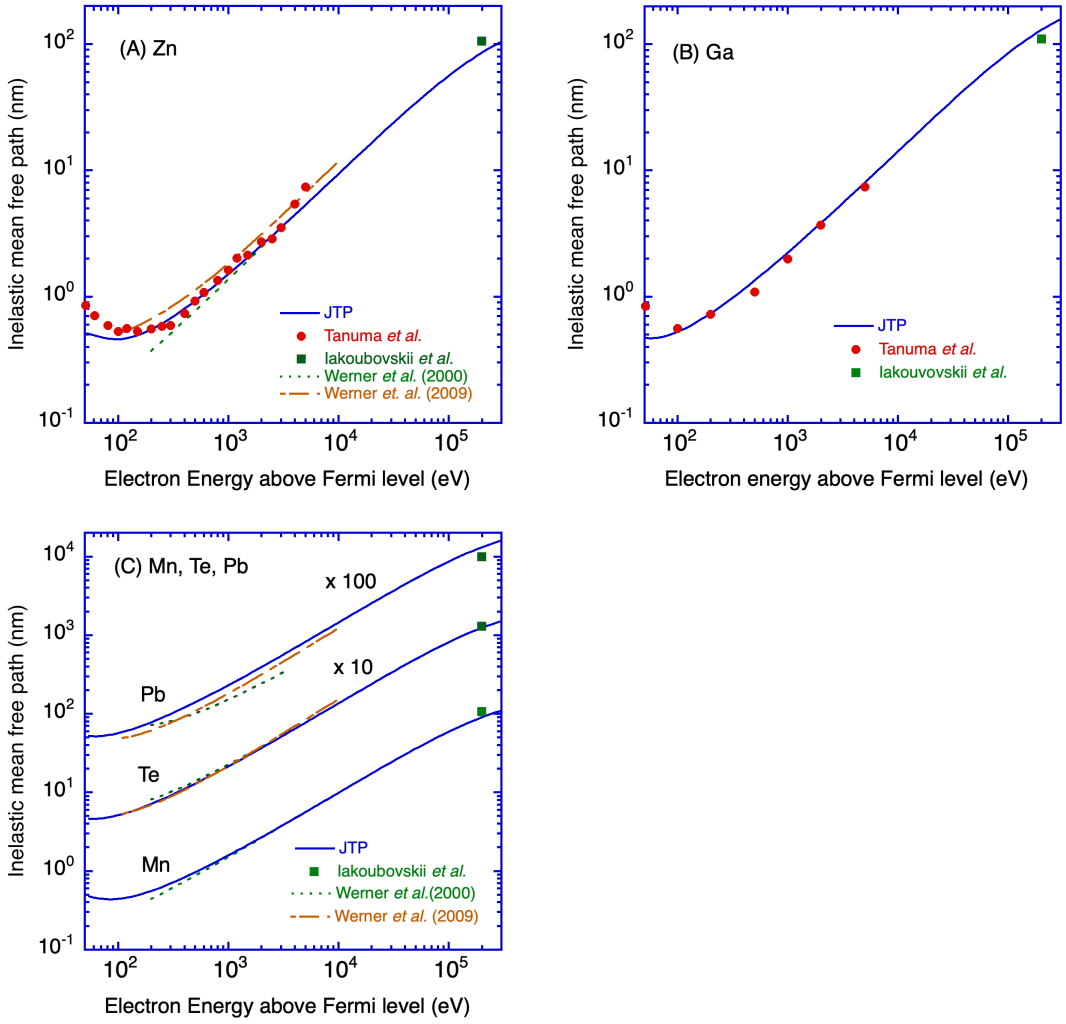

Figure 11. Comparisons of IMFPs calculated from the JTP equation (solid line, Eqs. 6 and 19) with the experimental IMFPs for (A) Zn, (B) Ga, and (C) Mn, Te, and Pb for energies between 50 eV and 200 keV. The solid lines show the IMFPs calculated from the JTP equation. The solid circles indicate IMFPs measured by Tanuma *et al.*[31] with EPES for energies between 50 eV and 5000 eV. The dotted lines show IMFPs calculated from the Bethe equation with parameters determined by Werner *et al.*[30] from EPES experiments for electron energies between 200 eV and 3400 eV. The solid squares indicate IMFPs measured by Iakoubovskii *et al.*[32] from TEM experiments at 200 keV. The long and short dashed lines show IMFPs calculated from Penn algorithm from optical ELF obtained from REELS measurement by Werner *et al.*[33]

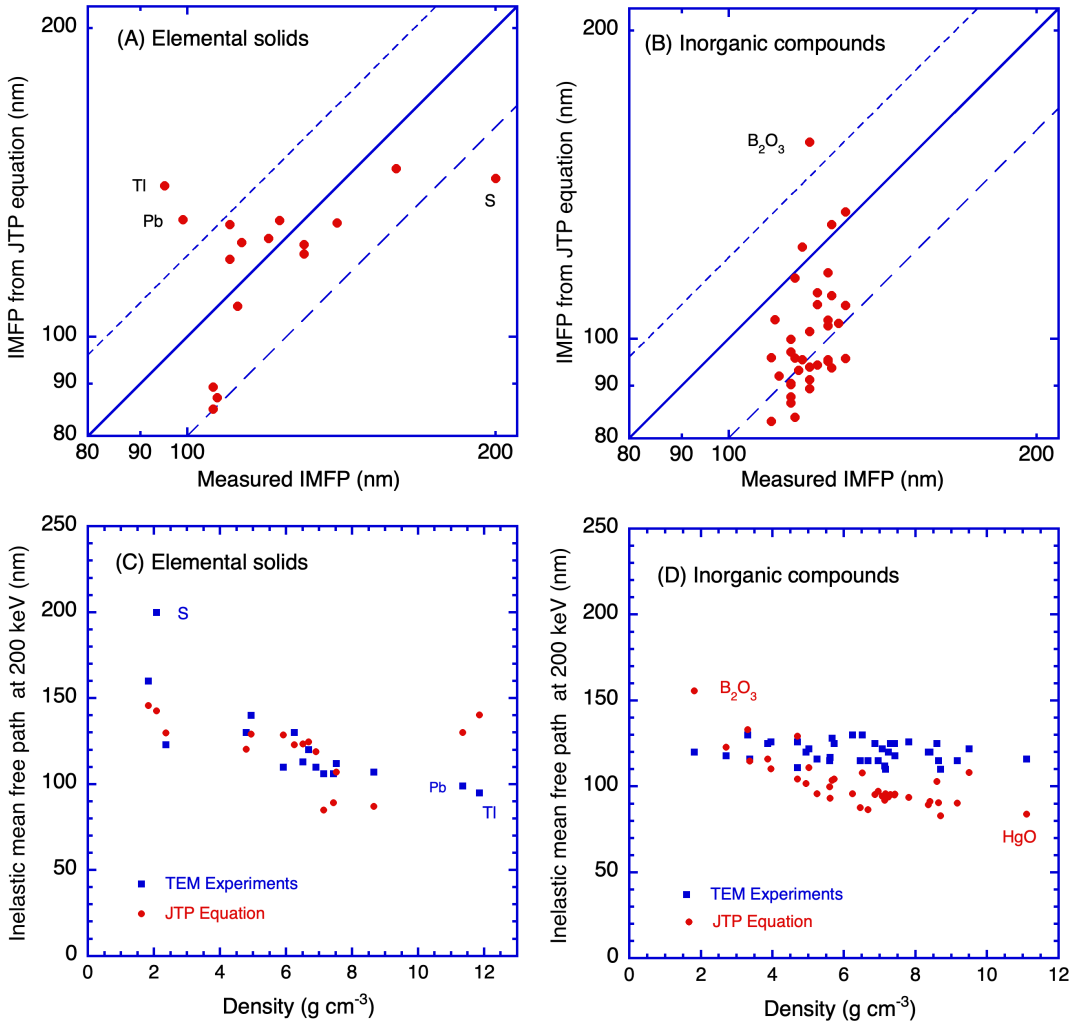

Figure 12. (A), (B): Plots of IMFPs calculated from the JTP equation versus IMFPs measured by Iakoubovskii *et al*. from TEM experiments at 200 keV for 16 elemental solids (A) and 37 inorganic compounds (B). The solid lines indicate perfect correlation between IMFPs from the JTP equation and measured IMFPs while the dashed lines indicate IMFPs that are 20 % larger and 20 % smaller than the calculated IMFPs. (C), (D): Plots of IMFPs from the JTP equation (JTP) and IMFPs from the TEM experiments of Iakoubovskii *et al.*[32] at 200 keV (TEM) as a function of density for the 16 elemental solids (C) and 37 inorganic compounds (D).

References

[1] ISO18115-1:2013(E) - Surface chemical analysis - Vocabulary - Part 1, General terms and terms used in spectroscopy. http://www.sasj.jp/iso/ISO18115.html

[2] Tanuma S, Powell CJ, Penn DR. Calculations of electron inelastic mean free paths. *Surf Interface Anal.* 1988; 11(11): 577-589. https://doi.org/10.1002/sia.740111107.

[3] Tanuma S, Powell CJ, Penn DR. Calculations of electron inelastic mean free paths. II. Data for 27 elements over the 50 – 2000 eV range. *Surf. Interface Anal.* 1991; 17(13): 911-926. https://doi.org/10.1002/sia.740171304.

[4] Tanuma S, Powell CJ, Penn DR. Calculations of electron inelastic mean free paths. III. Data for 15 inorganic compounds over the 50–2000 eV range. *Surf. Interface Anal.* 1991; 17(13): 927-939. https://doi.org/10.1002/sia.740171305.

[5] Tanuma S, Powell CJ, Penn DR. Calculations of electron inelastic mean free paths. V. Data for 14 organic compounds over the 50–2000 eV range. *Surf. Interface Anal.* 1994; 21(3): 165-176. https://doi.org/10.1002/sia.740210302.

[6] Penn DR. Electron mean-free-path calculations using a model dielectric function, *Phys. Rev. B.*1987; 35(2): 482-486. https://doi.org/10.1103/PhysRevB.35.482.

[7] Inokuti M. Inelastic collisions of fast charged particles with atoms and molecules – The Bethe theory revisited, *Rev. Mod. Phys.* 1971; 43: 297-347.

[8] Tanuma S, Powell CJ, Penn DR. Electron inelastic mean free paths in solids at low energies. *J. Electron Spectrosc. Relat. Phenom.* **1990**; 52: 285-291.

[9] Tanuma S, Powell CJ, Penn DR, Calculations of electron inelastic mean free paths. VIII. Data for 15 elemental solids over the 50 – 2000 eV range, *Surf. Interface Anal.* 2005; 37(1): 1-14. https://doi.org/10.1002/sia.1997.

[10] Powell CJ, Practical guide for inelastic mean free paths, effective attenuation lengths, mean escape depths, and information depths in x-ray photoelectron spectroscopy, *J. Vac. Sci. Technol.* A 38(2), 023209 (2020), https://doi.org/10.1116/1.5141079; erratum: *J. Vac. Sci. Technol.* A 38(5), 057001 (2020), 6.0000463.

[11] Tanuma S, Powell CJ, Penn DR, Calculations of electron inelastic mean free paths (IMFPs). VII. Reliability of the TPP-2M IMFP predictive equation, *Surf. Interface Anal.* 2003; 35: 268-275; https://doi.org/10.1002/sia.1526.

[12] Shinotsuka H, Tanuma S, Powell CJ, Penn DR. Calculations of electron inelastic mean free paths. X. Data for 41 elemental solids over the 50 eV to 200 keV range with the relativistic full Penn algorithm. Surf Interface Anal. 2015; 47: 871-888. https://doi.org/10.1002/sia.5789.

[13] Shinotsuka H, Tanuma S, Powell CJ, Penn DR. Calculations of electron inelastic mean free paths. XII. Data for 42 inorganic compounds over the 50 eV to 200 keV range with the full Penn algorithm. *Surf Interface Anal.* 2019; 51(4): 427-457. https://doi.org/10.1002/sia.6598.

[14] Shinotsuka H, Tanuma S, Powell CJ. Calculations of electron inelastic mean free paths. XIII. Data for 14 organic compounds and water over the 50 eV to 200 keV range with the relativistic full Penn algorithm. *Surf Interface Anal*. **2022**;54:534–560. doi:10.1002/sia.7064

[15] http://www.wien2k.at/; P. Blaha, K. Schwarz, G. K. H. Madsen, D. Kvasnicka, J. Luitz, WIEN2k, An Augmented Plane Wave + Local Orbitals Program for Calculating Crystal Properties (Karlheinz Schwarz, Tech. Universität Wien, Austria), 2001. ISBN 3-9501031-1-2.

[16] http://feffproject.org/; A. L. Ankudinov, C. Bouldin, J. J. Rehr, J. Sims, H. Hung, *Phys. Rev. B* 65, 104107 (2002).

[17] Boutboul T, Akkerman A, Breskin A, Chechik R. Electron inelastic mean free path and stopping power modelling in alkali halides in the 50 eV–10 keV energy range. *J. Appl. Phys.* 1996, 79, 6714.

[18] Lindhard J. ON THE PROPERTIES OF A GAS OF CHARGED PARTICLES. *Kgl. Danske Videnskab. Selskab Mat.-fys. Medd.*1954, 28, 1.

[19] Tanuma S, Powell CJ, Penn DR. Electron inelastic mean free paths in solids at low energies. *J. Electron Spectrosc. Relat. Phenom.* 1990; 52: 285-291.

[20] Rastrigin LA. About convergence of random search method in extremal control of multi-parameter systems, *Avtomat. i Telemekh*. 1963;24:1467-1473.

[21] Press WH, Teukolsky SA, Vetterling WT, Flannery BP. *Numerical recipes in Fortran 77. The art of scientific computing*, 2nd Edition, Cambridge University Press, Cambridge

(1992), p. 406.

[22] Frederikse HP, in *American Institute of Physics Handbook*, 3rd ed., edited by D. E. Gray (MsGraw Hill, New York, 1972), pp. 9-17.

[23] Strehlow WH, Cook EL. Compilation of Energy Band Gaps in Elemental and Binary Compound Semiconductors and Insulators. *J. Phys. Chem. Ref. Data* 1973;2: 163-193.

[24] Berger LI, in *CRC Handbook of Chemistry and Physics,* 95th ed., edited by W. M. Haynes (CRC, Boca Raton, 2014), pp. 12-90 to 12-99.

[25] Kittel C, *Introduction to Solid State Physics*, 6th ed. (Wiley, New York, 1986), p. 185.

[26] Wolke CM, Holonyak J, Stillman GE, *Physical Properties of Semiconductors* (Prentice-Hall, Englewood Cliffs, 1989).

[27] Seah MP. An accurate and simple universal curve for the energy-dependent electron inelastic mean free path, *Surface Interface Anal.* 2012;44;497-503

[28] Tanuma S, Powell CJ, Penn DR. Calculations of electron inelastic mean free paths. IX. Data for 41 elemental solids over the 50 eV to 30 keV range, *Surf. Interface Anal*. 2011; 43: 689 - 713.

[29] Liu Xun, Hou Zhufeng, Lu Dabao, B. Da Bo, Yoshikawa H, Tanuma S, Sun Yang, and Ding Zejun. Unveiling the principle descriptor for predicting the electron inelastic mean free path based on a machine learning framework, *Sci. Technol. Adv. Mater.* 2019; 20: 1090-1102.

[30] Werner WSM, Tomastik C, Cabela T, Richter G, Störi H. Electron inelastic mean free path measured by elastic peak electron spectroscopy for 24 solids between 50 and 3400 eV *Surf. Sci*. 2000; 470: L123-L128.

[31] Tanuma S, Shiratori T, Kimura T, Goto K, Ichimura S, Powell CJ. Experimental determination of electron inelastic mean free paths in 13 elemental solids in the 50 to 5000 eV energy range by elastic-peak electron spectroscopy, *Surf. Interface Anal*. 2005; 37: 833–845.

[32] Iakoubovskii K, Mitsuishi K, Nakayama Y, Furuya K. Mean free path of inelastic electron scattering in elemental solids and oxides using transmission electron microscopy: Atomic number dependent oscillatory behavior. *Phys. Rev. B* 2008; 77: 104102.

[33] Werner WSM, Glantschnig K, Ambrosch-Draxl C. Optical Constants and Inelastic Electron-Scattering Data for 17 Elemental Metals. *J. Phys. Chem. Ref. Data.* 2009; 38: 1013- 1092.

[34] http://www.esrf.fr/computing/scientific/dabax

[35] Palik ED. Handbook of Optical Constants of Solids I. New York: Academic Press; 1985.

[36] Cullen DE, Hubbell JH, Kissel L. EPDL97, The Evaluated Data Library, 1997 Version, UCRL-50400, Vol. 6, Rev. 5 (Sep 19, 1997). http://ftp.esrf.eu/pub/scisoft/xop2.3/DabaxFiles/

How to cite this article: Jablonski A, Tanuma S, Powell CJ. Calculations of electron inelastic mean free paths (IMFPs). XIV. Calculated IMFPs for LiF and Si3N4 and development of an improved predictive IMFP formula. Surf Interface Anal. 2023; 1-29. doi:10.1002/sia.7217